

Date repository materials for Paleomagnetism of the Late Ordovician Teel basalts of the Žavkhan Terrane – Paleozoic paleogeography of Mongolia

## Contents

|          |  |           |
|----------|--|-----------|
| <b>1</b> | <b>Teel Volcanics Paleomagnetic Data Analysis</b>                        | <b>1</b>  |
| 1.1      | Import Modules . . . . .   | 2         |
| 1.2      | Sampling localities . . . . .  | 2         |
| 1.3      | Site level data . . . . .  | 3         |
| 1.4      | Paleomagnetic site data summary . . . . .                                | 32        |
| 1.5      | Paleomagnetic Poles for the Teel Formation . . . . .                     | 46        |
| <b>2</b> | <b>Pole compilation for Siberia, North China, and Mongolian terranes</b> | <b>63</b> |
| 2.1      | Import existing paleomagnetic data . . . . .                             | 63        |
| 2.1.1    | Siberia . . . . .  | 63        |
| 2.1.2    | North China . . . . .  | 67        |
| 2.1.3    | Mongolia pole compilation . . . . .                                      | 68        |
| 2.2      | Paleolatitude diagram . . . . .  | 71        |
| <b>3</b> | <b>Regional overprints in Precambrian rocks</b>                          | <b>72</b> |
| <b>4</b> | <b>Data Repository References</b>  | <b>75</b> |

## 1 Teel Volcanics Paleomagnetic Data Analysis

This notebook is the data repository for a manuscript entitled:

**Paleomagnetism of the Late Ordovician Teel basalts of the Zavkhan Terrane – Paleozoic paleogeography of Mongolia**

T. M. Kilian, N. L. Swanson-Hysell, U. Bold, J. Crowley, and F. A. Macdonald

This manuscript is in review at the GSA journal *Lithosphere*.

This notebook contains data analysis related to paleomagnetic data generated from basalt flows of the Late Ordovician Teel Formation from the Zavkhan Terrane. The underlying data are available both within the MagIC Database and in the GitHub repository association with this work: [https://github.com/Swanson-Hysell-Group/2016\\_Teel\\_Basalts](https://github.com/Swanson-Hysell-Group/2016_Teel_Basalts)

## 1.1 Import Modules

Write template file (no\_code.tpl) so that when the notebook is converted to a latex (then pdf) it excludes the large code blocks. This requires an additional argument when using nbconveter and also requires that adding tables of content term after the document begins; can also add author. Can't include examples here because they affect the file when in latex.

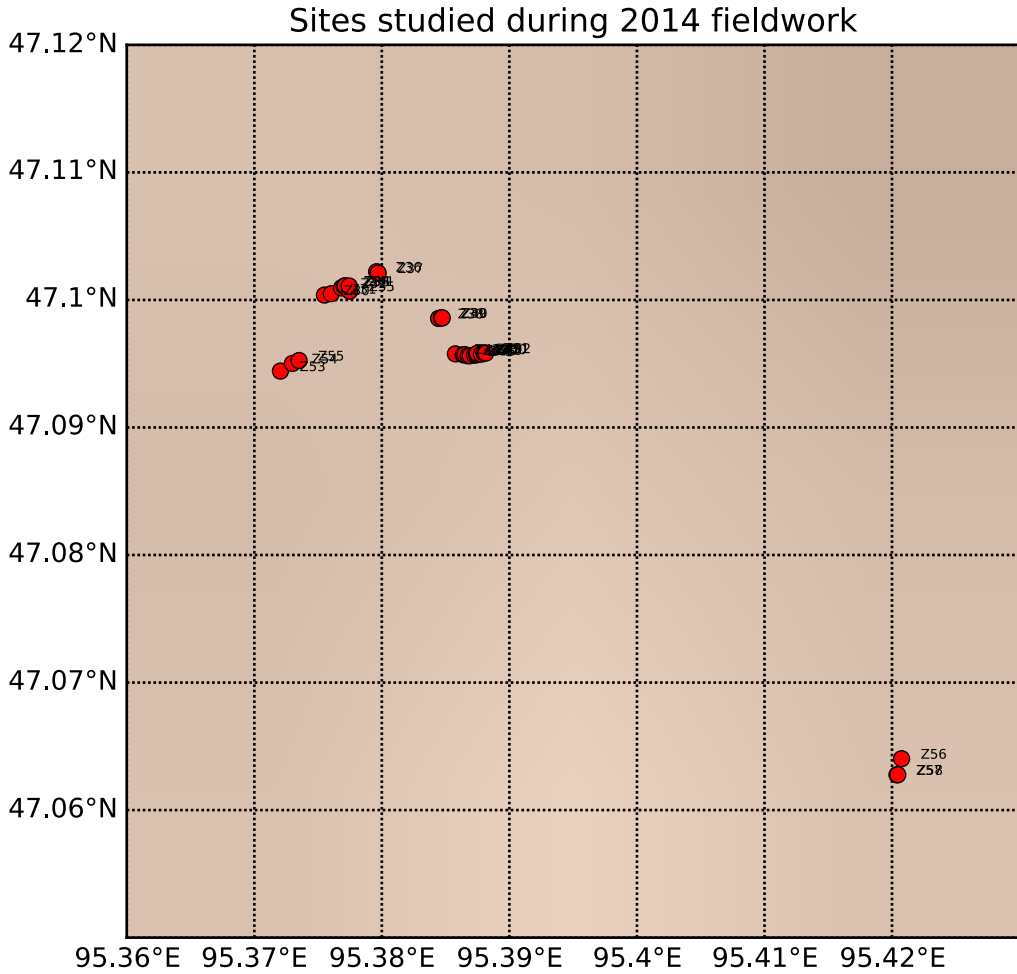
Overwriting no\_code\_latex.tplx

## 1.2 Sampling localities

Table of site locality coordinates given in WGS84 as well as a very simple map. Exact stratigraphic positions are shown in main text; order of stratigraphic position is given in “stat\_pos” column of table. The paleomagnetic data from these sites may need to be tilt-corrected (depending on the age of magnetization) according to nearby measurements of bedding. The bedding tilts used for sites Z30 to Z55 come from interflow sedimentary rocks. The tilt-corrections for Z56 to Z58 are more uncertain and are based on interpreted flow banding.

Out [5] :

|    | er_citation_names | er_location_name | er_site_name | site_lat | site_lon | strat_pos | sample_bed_dip_direction | sample_bed_dip |
|----|-------------------|------------------|--------------|----------|----------|-----------|--------------------------|----------------|
| 0  | This study        | Khukh_Davaa      | Z30          | 47.10038 | 95.37550 | 4.0       | 88                       | 58             |
| 1  | This study        | Khukh_Davaa      | Z31          | 47.10049 | 95.37604 | 5.0       | 88                       | 58             |
| 2  | This study        | Khukh_Davaa      | Z32          | 47.10094 | 95.37684 | 6.0       | 84                       | 55             |
| 3  | This study        | Khukh_Davaa      | Z33          | 47.10107 | 95.37705 | 7.0       | 84                       | 55             |
| 4  | This study        | Khukh_Davaa      | Z34          | 47.10111 | 95.37712 | 8.0       | 84                       | 55             |
| 5  | This study        | Khukh_Davaa      | Z35          | 47.10069 | 95.37747 | 9.0       | 84                       | 55             |
| 6  | This study        | Khukh_Davaa      | Z36          | 47.10221 | 95.37959 | 11.0      | 89                       | 47             |
| 7  | This study        | Khukh_Davaa      | Z37          | 47.10211 | 95.37971 | 12.0      | 89                       | 47             |
| 8  | This study        | Khukh_Davaa      | Z38          | 47.09855 | 95.38445 | 13.0      | 87                       | 46             |
| 9  | This study        | Khukh_Davaa      | Z39          | 47.09860 | 95.38467 | 14.0      | 87                       | 46             |
| 10 | This study        | Khukh_Davaa      | Z40          | 47.09859 | 95.38474 | 15.0      | 87                       | 46             |
| 11 | This study        | Khukh_Davaa      | Z41          | 47.10109 | 95.37744 | 10.0      | 84                       | 55             |
| 12 | This study        | Khukh_Davaa      | Z42          | 47.09577 | 95.38577 | 16.0      | 87                       | 37             |
| 13 | This study        | Khukh_Davaa      | Z43          | 47.09570 | 95.38638 | 17.0      | 87                       | 37             |
| 14 | This study        | Khukh_Davaa      | Z44          | 47.09571 | 95.38651 | 18.0      | 87                       | 37             |
| 15 | This study        | Khukh_Davaa      | Z45          | 47.09562 | 95.38676 | 19.0      | 87                       | 37             |
| 16 | This study        | Khukh_Davaa      | Z46          | 47.09563 | 95.38692 | 20.0      | 87                       | 37             |
| 17 | This study        | Khukh_Davaa      | Z47          | 47.09568 | 95.38727 | 21.0      | 87                       | 37             |
| 18 | This study        | Khukh_Davaa      | Z48          | 47.09570 | 95.38744 | 22.0      | 91                       | 28             |
| 19 | This study        | Khukh_Davaa      | Z49          | 47.09581 | 95.38747 | 23.0      | 91                       | 28             |
| 20 | This study        | Khukh_Davaa      | Z50          | 47.09575 | 95.38781 | 24.0      | 91                       | 28             |
| 21 | This study        | Khukh_Davaa      | Z51          | 47.09584 | 95.38802 | 25.0      | 91                       | 28             |
| 22 | This study        | Khukh_Davaa      | Z52          | 47.09583 | 95.38815 | 26.0      | 91                       | 28             |
| 23 | This study        | Khukh_Davaa      | Z53          | 47.09442 | 95.37205 | 1.0       | 88                       | 58             |
| 24 | This study        | Khukh_Davaa      | Z54          | 47.09502 | 95.37299 | 2.0       | 88                       | 58             |
| 25 | This study        | Khukh_Davaa      | Z55          | 47.09525 | 95.37351 | 3.0       | 88                       | 58             |
| 26 | This study        | Khukh_Davaa      | Z56          | 47.06403 | 95.42075 | NaN       | 165                      | 24             |
| 27 | This study        | Khukh_Davaa      | Z57          | 47.06277 | 95.42039 | NaN       | 165                      | 24             |
| 28 | This study        | Khukh_Davaa      | Z58          | 47.06277 | 95.42045 | NaN       | 165                      | 24             |

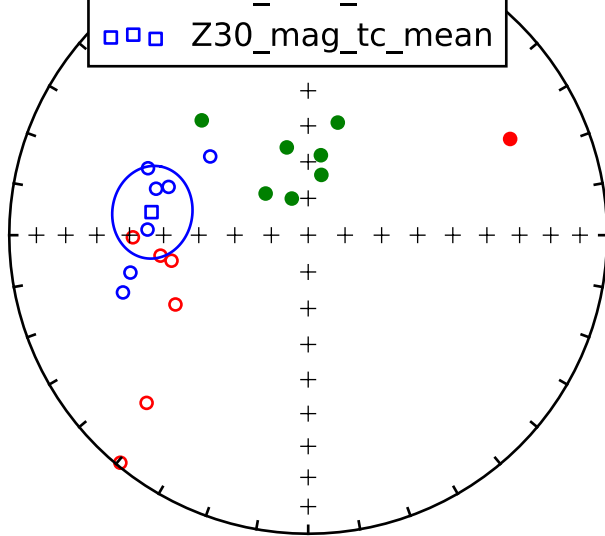


### 1.3 Site level data

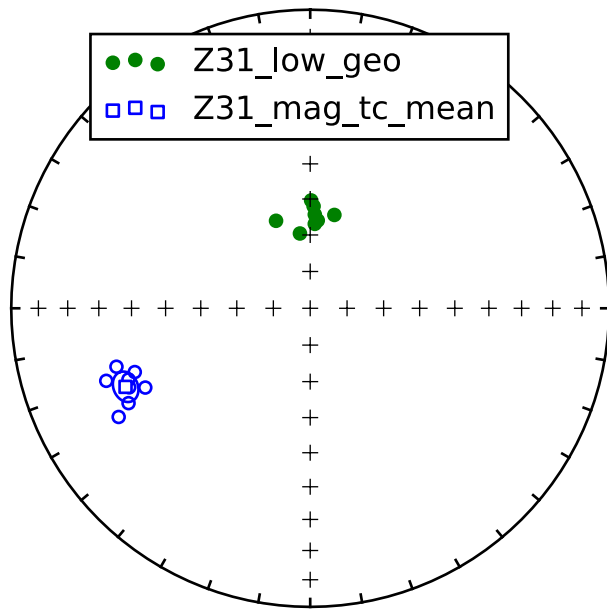
Below we import paleomagnetic results that were analyzed using demag-gui.py from the PmagPy python package. These are the vector component fits to all Teel sample data. Components have been classified according to their relative temperature ranges. ‘LOW’ components are typically below 200°C, ‘MAG’ refers to a temperature range within the unblocking range of magnetite (up to 580°C), ‘HEM’ refers to vector components fit to data points in the unblocking range of hematite (up to 680°C), and ‘MID’ refers to components with temperature ranges between ‘LOW’ and ‘MAG’.

**Z30** Site Z30 is a rhyolite. The site has ‘LOW’, ‘MAG’ and poorly resolved ‘HEM’ components.

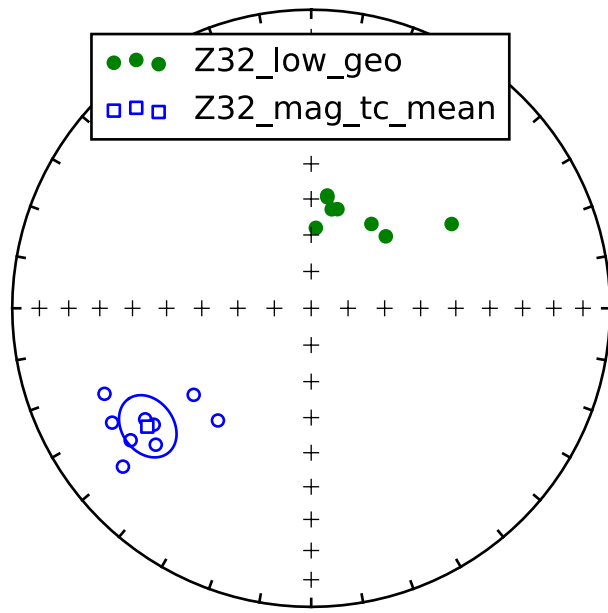
●●● Z30\_low\_geo  
○○○ Z30\_hem\_tc  
●●● Z30\_hem\_tc  
□□□ Z30\_mag\_tc\_mean



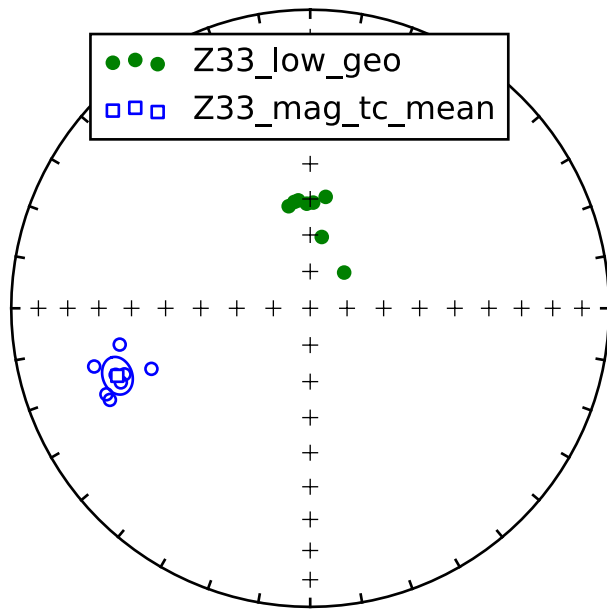
**Z31** The site has ‘LOW’ (less than 200°C) and ‘MAG’ components.



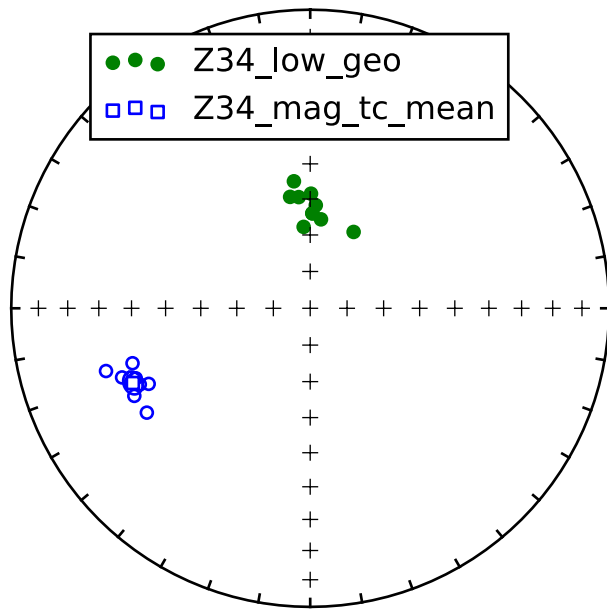
**Z32** The site has ‘LOW’ (less than 200°C) and ‘MAG’ components.



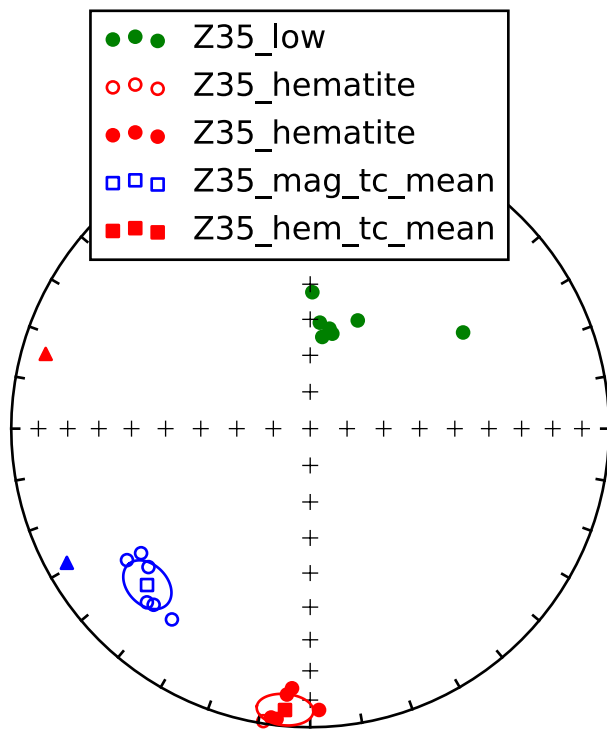
**Z33** The site has ‘LOW’ (less than 200°C) and ‘MAG’ components.



**Z34** The site has ‘LOW’ (less than 200°C) and ‘MAG’ components.

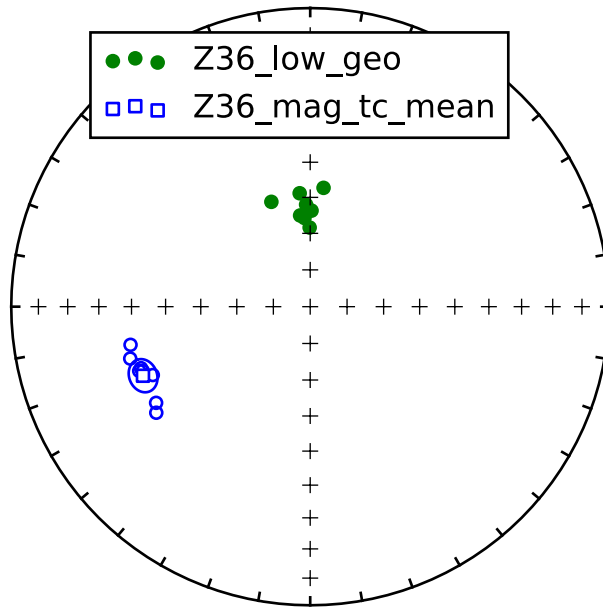


**Z35** The site has ‘LOW’, ‘MAG’ and ‘HEM’ components.

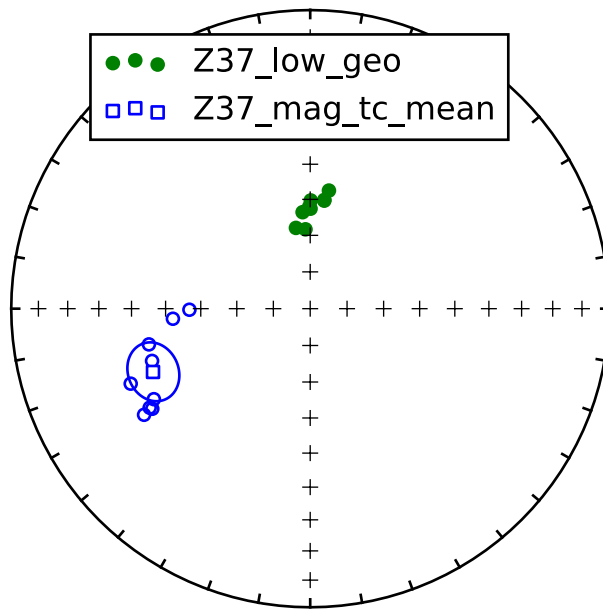


Data points shown with triangles were vectors from sample Z35.3 that were dropped from the mean calculation.

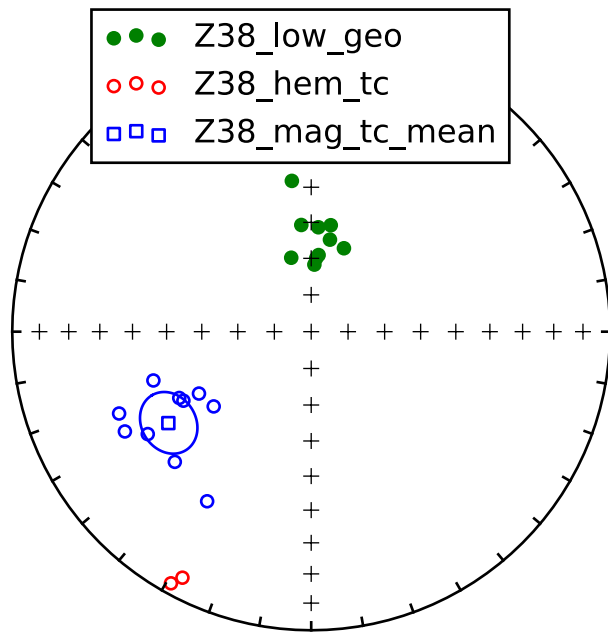
**Z36** The site has ‘LOW’ and ‘MAG’ components.



**Z37** The site has ‘LOW’ and ‘MAG’ components.

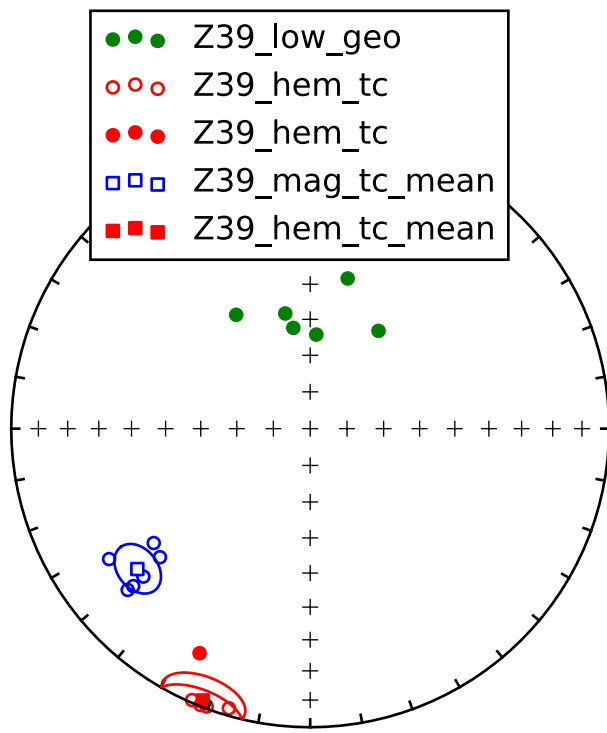


**Z38** The site has ‘LOW’, ‘MAG’ and ‘HEM’ components.

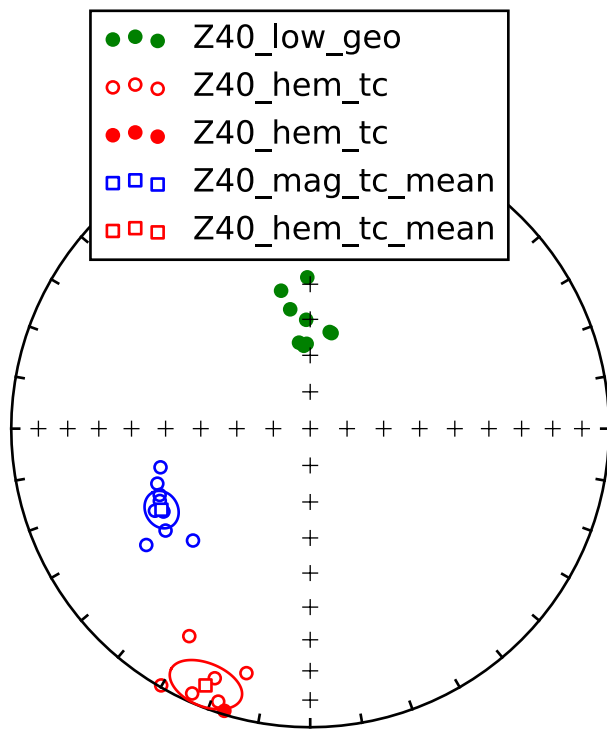


Only two samples yielded hematite components, therefore no mean was calculated for the hematite component.

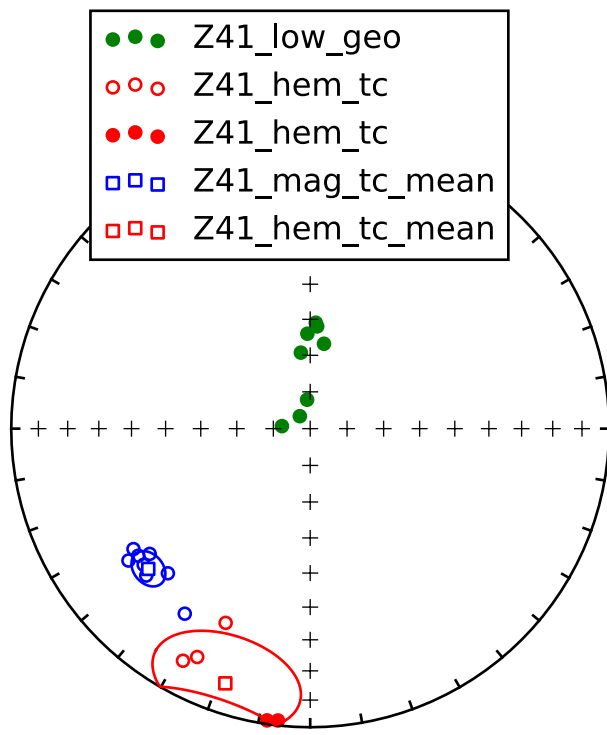
**Z39** The site has 'LOW', 'MAG' and 'HEM' components.



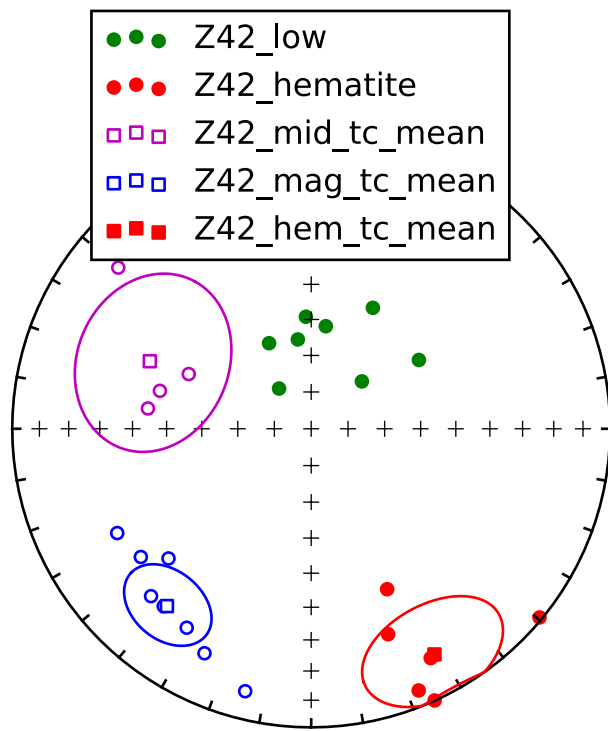
**Z40** The site has 'LOW', 'MAG' and 'HEM' components.



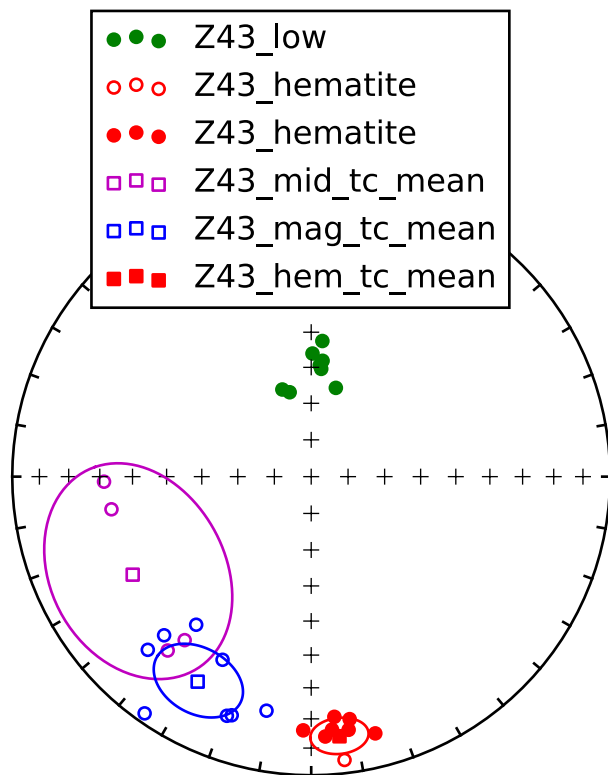
**Z41** The site has 'LOW', 'MAG' and 'HEM' components.



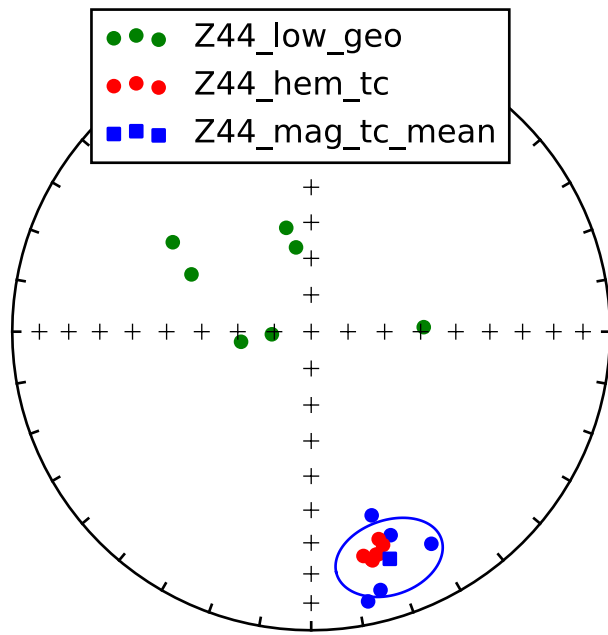
**Z42** The site has ‘LOW’, ‘MAG’ and ‘HEM’ components. A middle temperature component, MID, was also fit to demagnetization steps between ‘LOW’ and ‘MAG’.



**Z43** The site has ‘LOW’, ‘MAG’ and ‘HEM’ components. A middle temperature component, MID, was also fit to demagnetization steps between ‘LOW’ and ‘MAG’.

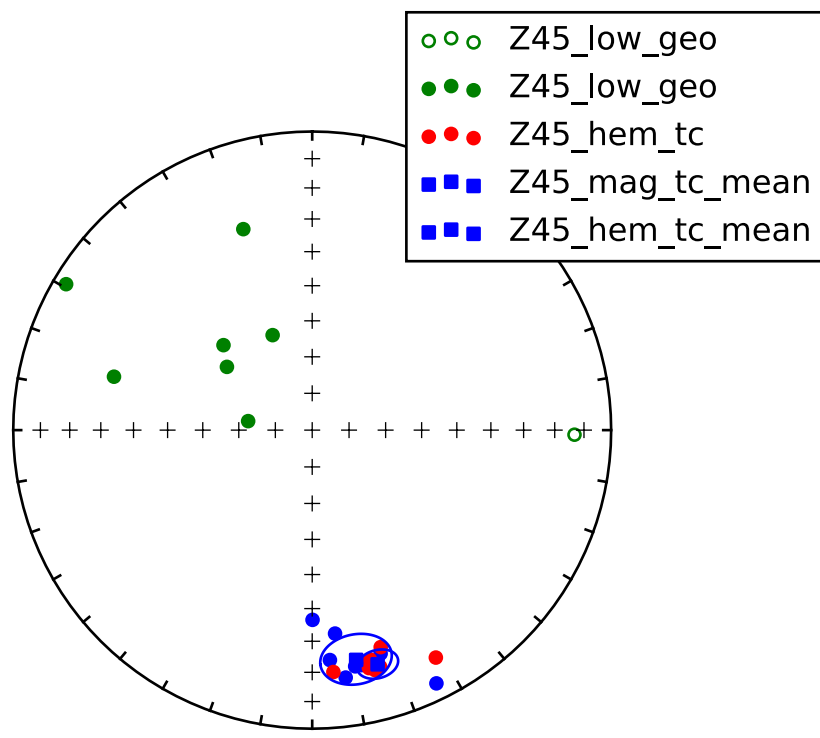


**Z44** The site has ‘LOW’, ‘MAG’ and ‘HEM’ components.



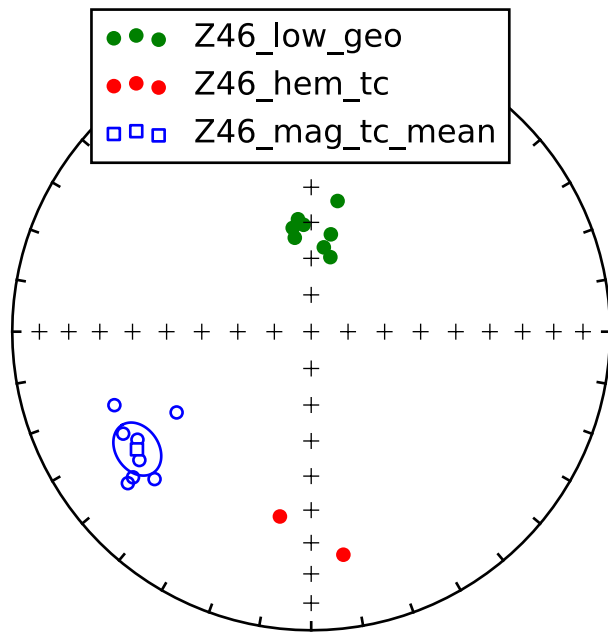
The remanence of Z44 specimens is dominated by hematite such that the magnetite component is poorly resolved.

**Z45** Hematite, magnetite, and low temperature, LOW (less than 200°C), components were calculated for Z45.

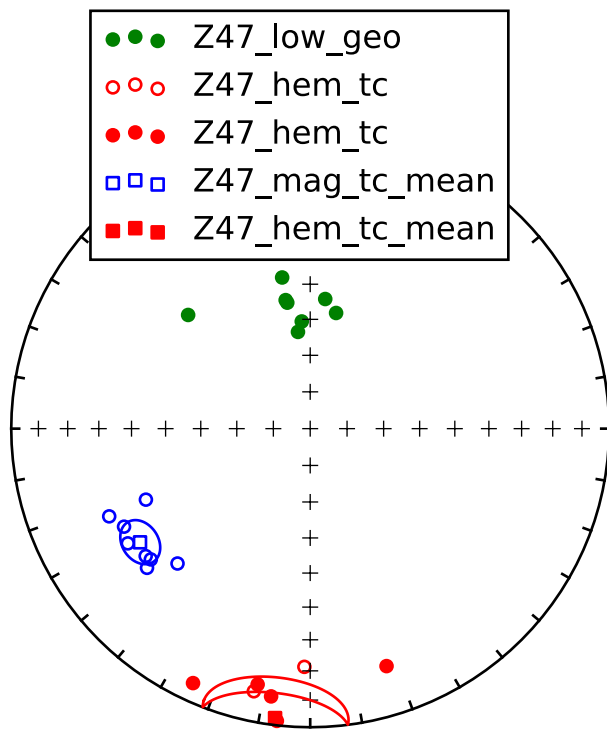


The remanence of Z45 specimens is dominated by hematite such that the magnetite component is poorly resolved.

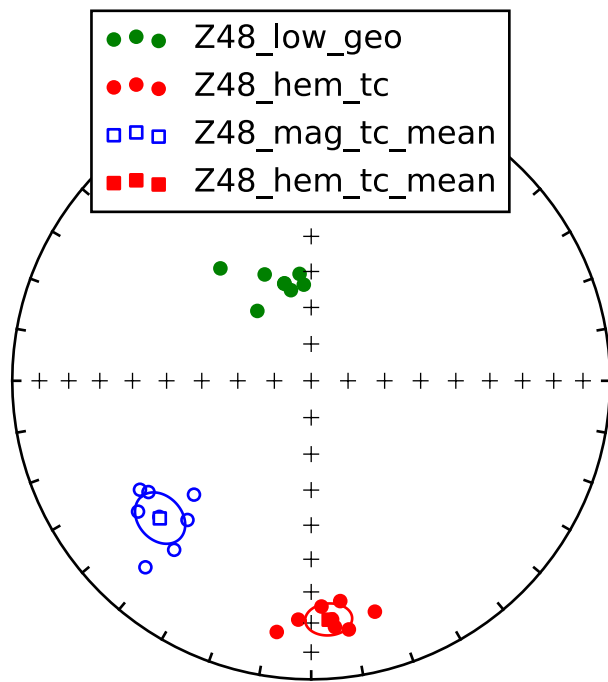
**Z46** The site has 'LOW', 'MAG' and 'HEM' components.



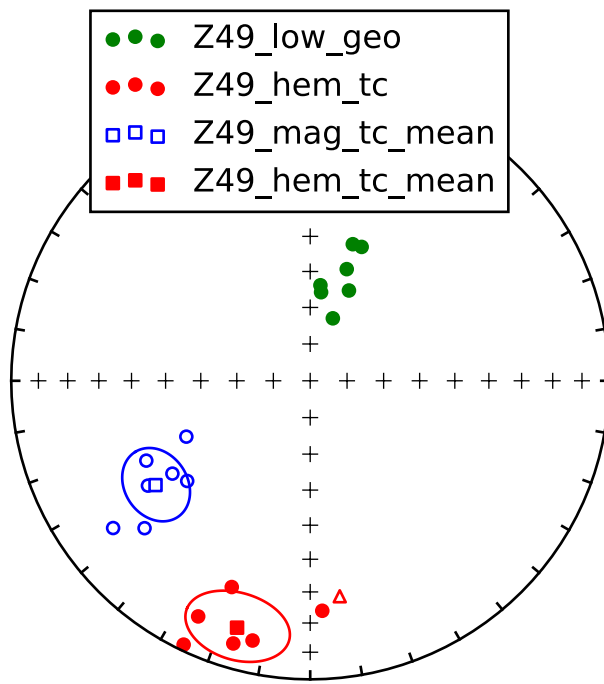
**Z47** The site has 'LOW', 'MAG' and 'HEM' components.



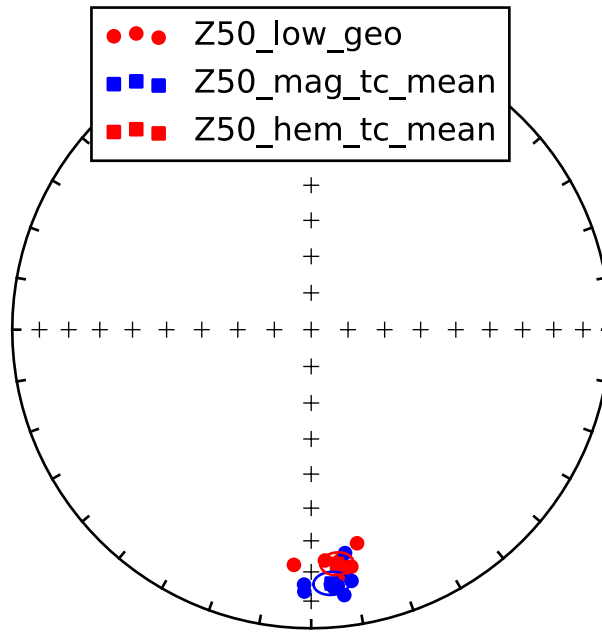
**Z48** The site has 'LOW', 'MAG' and 'HEM' components.



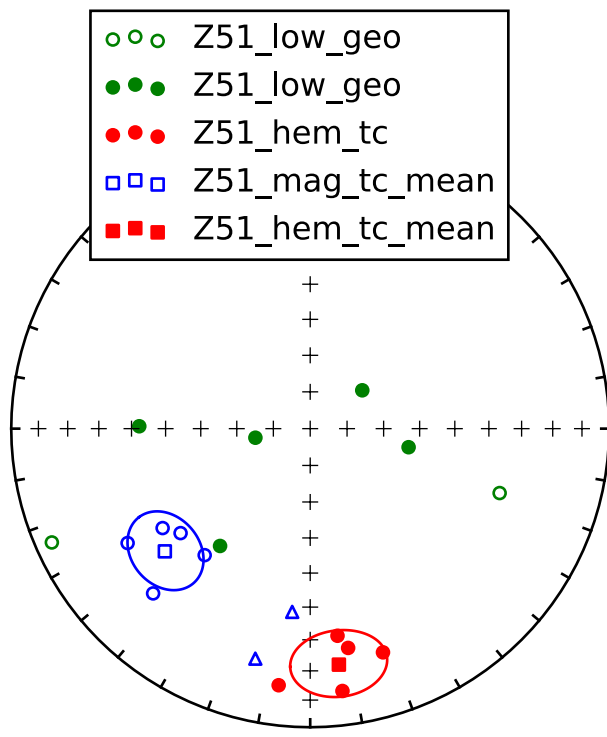
**Z49** The site has 'LOW', 'MAG' and 'HEM' components.



**Z50** The site has ‘MAG’ and ‘HEM’ components.

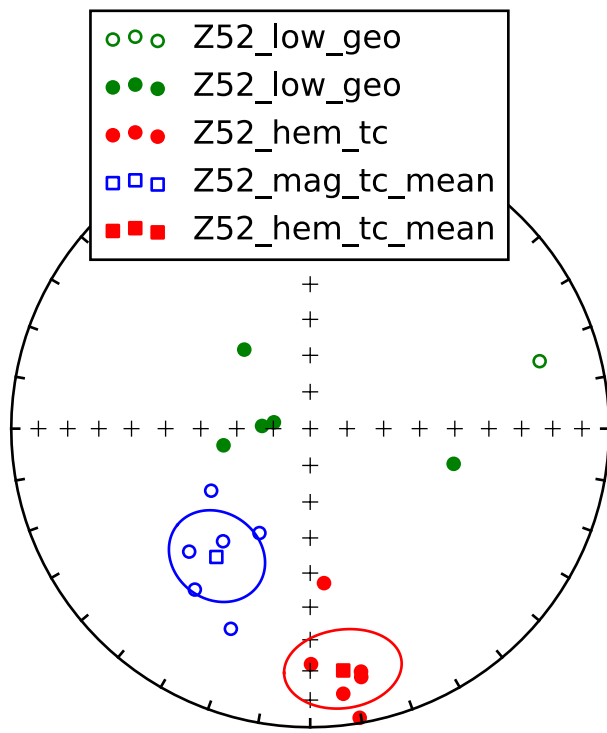


**Z51** The site has ‘LOW’, ‘MAG’ and ‘HEM’ components.

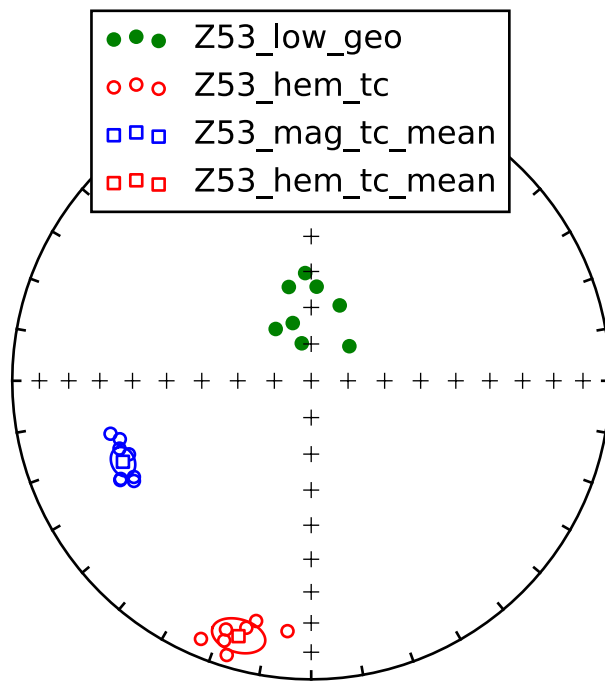


Magnetite components from two samples (Z51.1 and Z51.2) were excluded because of their similarity to hematite components (the hematite remanence mixed with that of magnetite) and different demagnetization behavior compared to the other magnetite components.

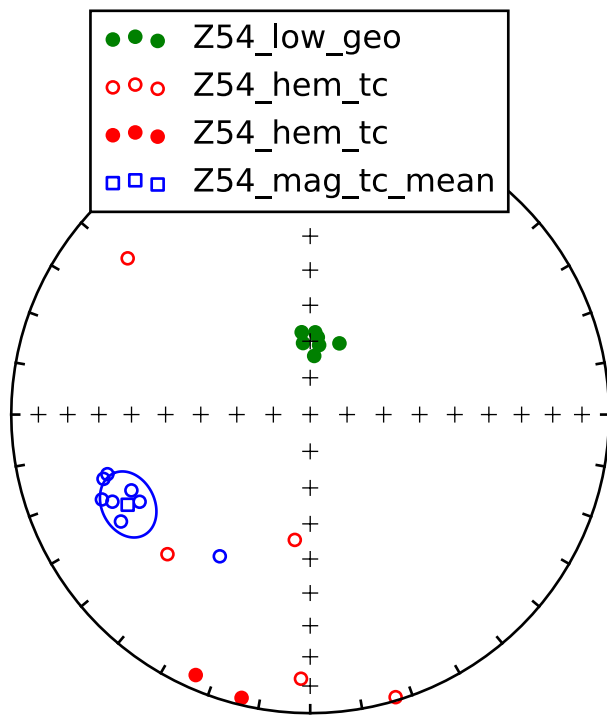
**Z52** The site has 'LOW', 'MAG' and 'HEM' components.



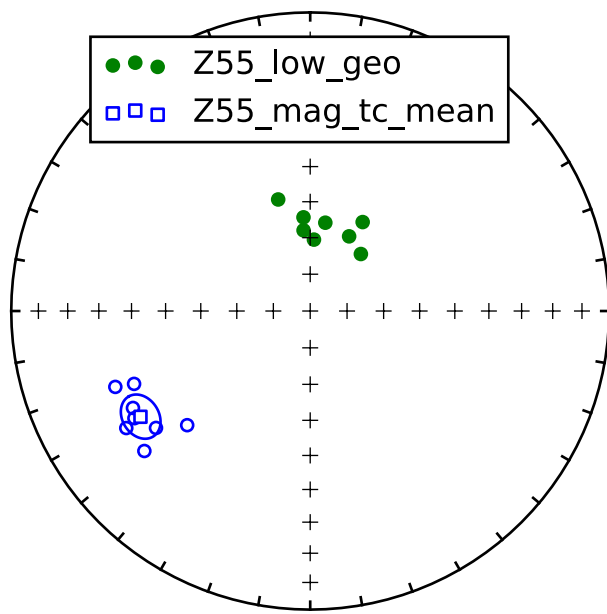
**Z53** The site has 'LOW', 'MAG' and 'HEM' components.



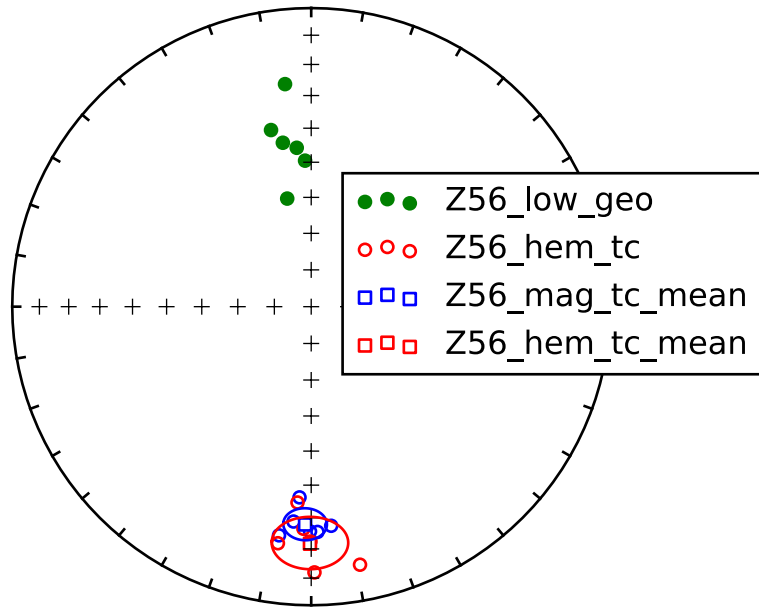
**Z54** The site has 'LOW', 'MAG' and 'HEM' components.



**Z55** The site has 'LOW' and 'MAG'.

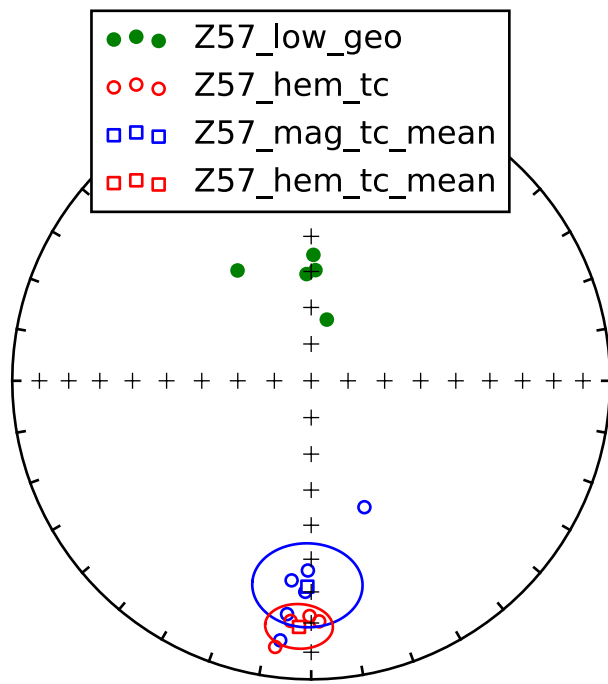


**Z56** The site has ‘LOW’, ‘MAG’ and ‘HEM’ components.

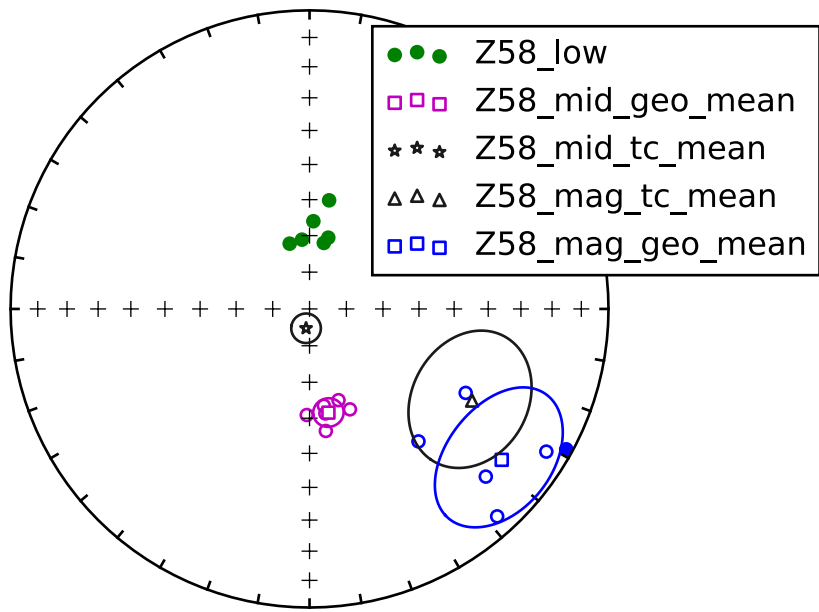


This site is in a different dip panel along with Z57 and Z58. A magnetite component distinct from the hematite component was not resolved. Z57 has similar behavior.

**Z57** The site has ‘LOW’, ‘MAG’ and ‘HEM’ components.



**Z58** Magnetite, mid-, and low- temperature, LOW (less than 200°C), components were calculated for Z58. The middle temperature component derives from demagnetization steps between LOW and magnetite.



Results from flow Z58 are very different from all of the other sites.

#### 1.4 Paleomagnetic site data summary

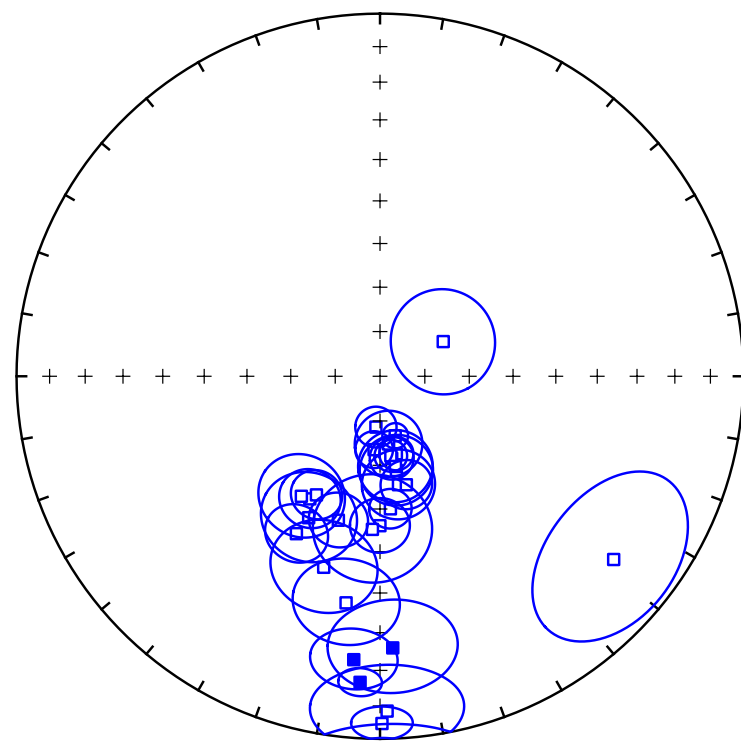
Create tables, distinguished by component type, of mean directions for all Teel flows.

##### Magnetite directions

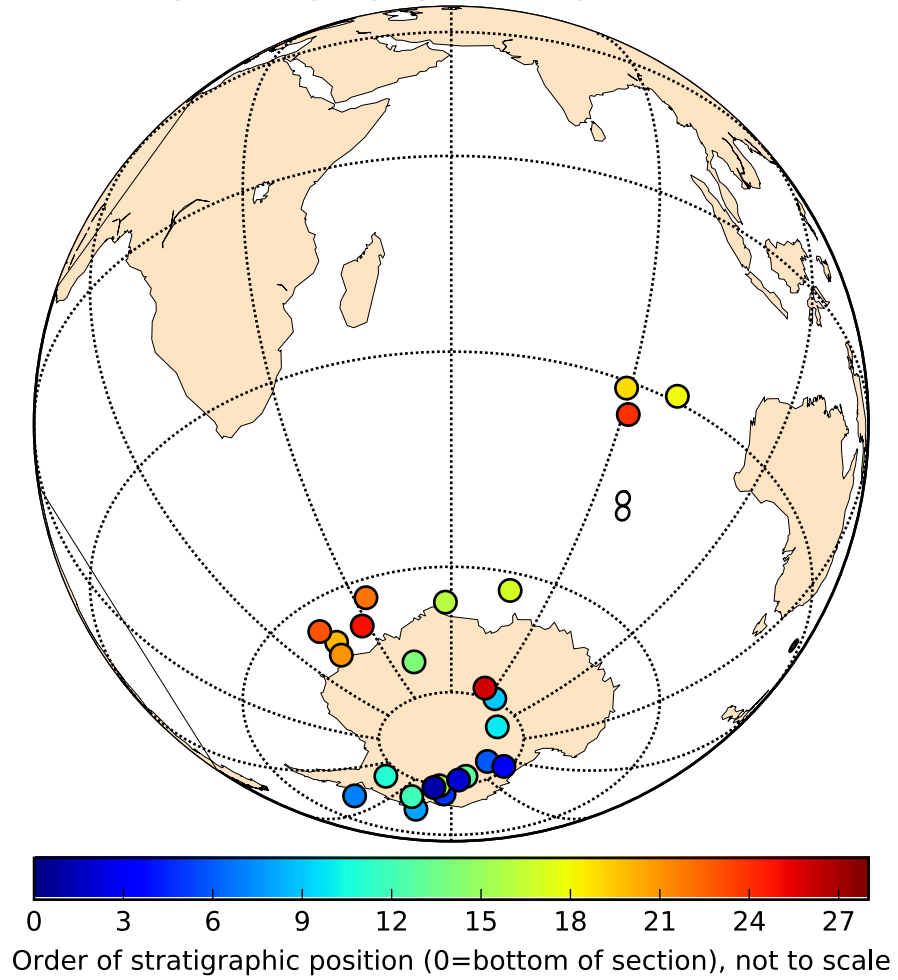
Geographic coordinates - magnetite Out [66]:

|             | strat_pos | site_lat | site_lon | dec_geo    | inc_geo     | alpha95    | n          | k          | r        | csd        | paleolatitude | vgp_lat    | vgp_lon    | vgp_lat_rev | vgp_lon_rev |
|-------------|-----------|----------|----------|------------|-------------|------------|------------|------------|----------|------------|---------------|------------|------------|-------------|-------------|
| Z30_mag-geo | 4.0       | 47.10038 | 95.37550 | 61.199035  | -73.861110  | 11.712582  | 7          | 27.513985  | 6.781929 | 15.4412168 | -59.940264    | -28.018244 | 245.555936 | 65.555956   |             |
| Z31_mag-geo | 5.0       | 47.10049 | 95.37604 | 168.103623 | -72.234668  | 3.753459   | 8          | 218.756351 | 7.968001 | 5.476520   | -57.348450    | -77.463763 | 244.552326 | 64.552326   |             |
| Z32_mag-geo | 6.0       | 47.10094 | 95.37684 | 170.358827 | -65.228366  | 7.987595   | 9          | 42.504477  | 8.811785 | 12.424178  | -47.295204    | -83.450449 | 190.612182 | 83.450449   |             |
| Z33_mag-geo | 7.0       | 47.10107 | 95.37705 | 184.611118 | -78.580341  | 4.579774   | 8          | 147.251468 | 7.952462 | 6.675060   | -68.002034    | -68.966892 | 280.189099 | 100.189099  |             |
| Z34_mag-geo | 8.0       | 47.10111 | 95.37712 | 165.710954 | -76.241270  | 2.846954   | 10         | 288.897760 | 9.968847 | 4.765549   | -63.908090    | -71.445651 | 255.430852 | 75.430852   |             |
| Z35_mag-geo | 9.0       | 47.10069 | 95.37747 | 180.035625 | -56.117492  | 6.392221   | 6          | 110.823428 | 5.954883 | 7.694302   | -36.670242    | -79.569519 | 95.219636  | 275.219636  |             |
| Z36_mag-geo | 11.0      | 47.10221 | 95.37959 | 184.602274 | -73.48365   | 4.160116   | 8          | 178.256399 | 7.960731 | 6.066839   | -59.330031    | -77.472930 | 286.256471 | 106.256471  |             |
| Z37_mag-geo | 12.0      | 47.10211 | 95.37971 | 172.808147 | -74.694707  | 7.476051   | 9          | 48.384817  | 8.834659 | 11.644758  | -61.306496    | -75.207168 | 261.763513 | 81.763513   |             |
| Z38_mag-geo | 13.0      | 47.09855 | 95.38445 | 170.143849 | -68.504682  | 8.040139   | 10         | 37.061501  | 9.757160 | 13.305265  | -51.774894    | -82.07705  | 225.175390 | 45.175390   |             |
| Z39_mag-geo | 14.0      | 47.09860 | 95.38467 | 196.103583 | -56.020236  | 6.360400   | 6          | 111.925588 | 5.955327 | 7.656324   | -36.571555    | -74.094885 | 221.007252 | 69.100583   |             |
| Z40_mag-geo | 15.0      | 47.09859 | 95.38474 | 171.882175 | -71.414505  | 4.837145   | 9          | 114.250096 | 8.929978 | 7.578037   | -56.078745    | -79.716310 | 249.190533 | 79.716310   |             |
| Z41_mag-geo | 10.0      | 47.10109 | 95.37744 | 175.528989 | -59.942821  | 4.580179   | 8          | 147.225628 | 7.952454 | 6.675646   | -40.828095    | -82.952676 | 124.113660 | 82.952676   |             |
| Z42_mag-geo | 16.0      | 47.09577 | 95.38577 | 196.391432 | -44.308602  | 11.150650  | 8          | 25.632057  | 7.726904 | 15.999017  | -26.015899    | -65.239739 | 58.086778  | 65.239739   |             |
| Z43_mag-geo | 17.0      | 47.09570 | 95.38638 | 188.500123 | -36.936066  | 10.749181  | 8          | 25.509395  | 7.745546 | 15.443305  | -20.601392    | -62.620370 | 57.877325  | 62.620370   |             |
| Z44_mag-geo | 18.0      | 47.09571 | 95.38651 | 177.320106 | -25.952966  | 12.3333051 | 5          | 39.443485  | 4.898589 | 12.897258  | 13.6777537    | -29.179269 | 98.369133  | 278.369133  |             |
| Z45_mag-geo | 19.0      | 47.09572 | 95.38672 | 185.281245 | 22.577189   | 8.142853   | 8          | 47.231012  | 7.851792 | 11.786134  | 11.744294     | -30.970825 | 89.353703  | 269.353703  |             |
| Z46_mag-geo | 20.0      | 47.09563 | 95.38692 | 209.744992 | -58.036511  | 6.728483   | 8          | 68.732448  | 7.889155 | 9.770236   | -38.705303    | -66.823872 | 15.721243  | 66.823872   |             |
| Z47_mag-geo | 21.0      | 47.09568 | 95.38727 | 208.133979 | -59.587799  | 5.606451   | 8          | 98.575940  | 7.928989 | 8.158298   | -68.748397    | -13.361225 | 68.748397  | 193.361225  |             |
| Z48_mag-geo | 22.0      | 47.09574 | 95.38744 | 207.921657 | -49.345412  | 6.760918   | 8          | 68.092935  | 7.897184 | 9.816705   | -30.209549    | -62.672462 | 33.563539  | 62.672462   |             |
| Z49_mag-geo | 23.0      | 47.09581 | 95.38747 | 213.177701 | -57.526629  | 9.488165   | 7          | 41.429419  | 6.895175 | 12.583435  | -38.154890    | -64.243434 | 13.523120  | 64.243434   |             |
| Z50_mag-geo | 24.0      | 47.09575 | 95.38781 | 183.717358 | 16.532802   | 3.910452   | 8          | 201.610149 | 7.965281 | 5.704520   | 8.442107      | -34.363744 | 90.931921  | 34.363744   |             |
| Z51_mag-geo | 25.0      | 47.09584 | 95.38802 | 206.717692 | -54.030732  | 10.393862  | 5          | 55.146896  | 4.927466 | 10.907481  | -34.565590    | -66.394972 | 27.782142  | 66.394972   |             |
| Z52_mag-geo | 26.0      | 47.09583 | 95.38815 | 182.85182  | -65.213178  | 12.719642  | 6          | 28.697188  | 5.825767 | 15.120472  | -35.744789    | -78.453731 | 83.87965   | 263.87965   |             |
| Z53_mag-geo | 1.0       | 47.09442 | 95.37205 | 172.278467 | -3.594132   | 8          | 238.494787 | 7.970649   | 5.245001 | -56.957385 | -252.646197   | 72.646197  | 72.646197  |             |             |
| Z54_mag-geo | 2.0       | 47.09502 | 95.37299 | 170.318109 | -69.953189  | 8.193477   | 8          | 46.660914  | 7.849982 | 11.857917  | -53.143586    | -81.346675 | 233.270089 | 81.346675   |             |
| Z55_mag-geo | 3.0       | 47.09525 | 95.37351 | 166.338653 | -64.1854630 | 5.625088   | 8          | 97.930102  | 7.928520 | 8.185155   | -46.807981    | -80.714545 | 188.593646 | 8.593646    |             |
| Z56_mag-geo | NaN       | 47.06403 | 95.42075 | 179.680351 | -4.756236   | 5.057226   | 6          | 176.489683 | 5.971670 | 6.097129   | -2.38222      | -45.317329 | 95.874936  | 275.874936  |             |
| Z57_mag-geo | NaN       | 47.06277 | 95.42039 | 178.736826 | -8.456342   | 13.052562  | 6          | 27.299686  | 5.816848 | 15.502659  | -4.251323     | -47.175716 | 97.200362  | 277.200362  |             |
| Z58_mag-geo | NaN       | 47.06277 | 95.42045 | 128.167765 | -19.352349  | 17.533117  | 6          | 15.552391  | 5.678506 | 20.533938  | -9.960183     | -32.768009 | 342.478280 | 32.768009   |             |

High-temperature magnetite (geographic) directions for Teel basalt flows



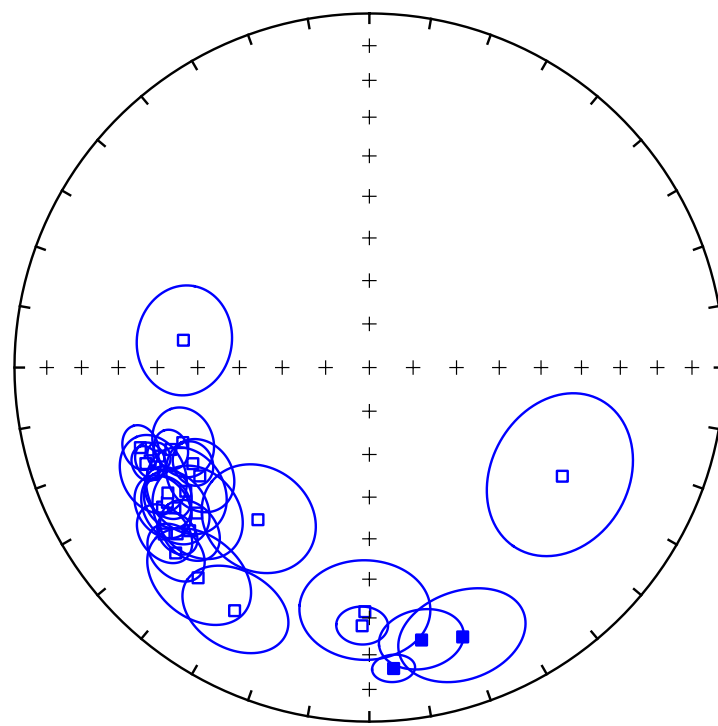
### Magnetite (geographic) component VGPs



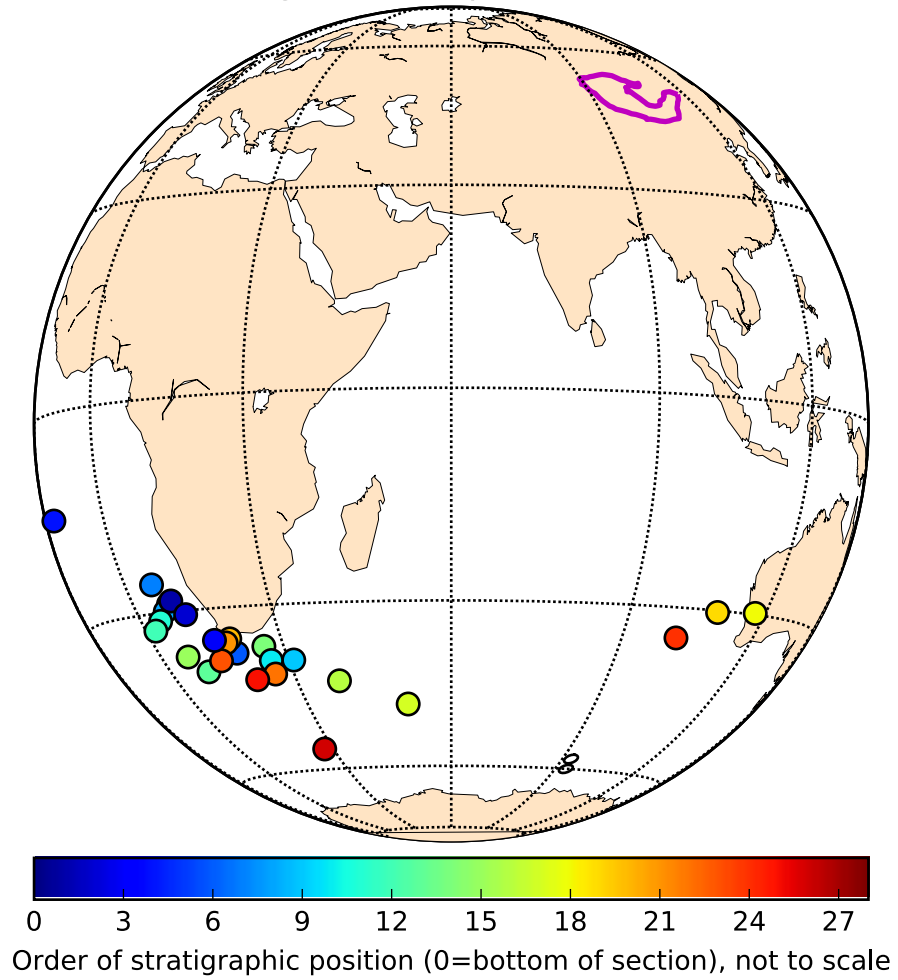
Tilt-corrected coordinates - magnetite Out[69]:

| strat-pos | site_lat | site_lon   | dec_tc     | inc_tc      | alpha95    | n         | k          | r          | csd       | paleolatitude | vgp_lat    | vgp_lon    | vgp_lat_rev | vgp_lon_rev |
|-----------|----------|------------|------------|-------------|------------|-----------|------------|------------|-----------|---------------|------------|------------|-------------|-------------|
| Z30_mag   | 4.0      | 47.10038   | 95.37550   | 278.379367  | -46.010280 | 11.715664 | 7          | 27.500112  | 6.781818  | 15.446091     | -27.381947 | -14.408220 | 340.470733  | 160.470733  |
| Z31_mag   | 5.0      | 47.10049   | 95.37604   | 246.928601  | -33.319165 | 3.753646  | 8          | 218.734693 | 7.967998  | 5.476791      | -18.194560 | -28.826591 | 9.314505    | 189.314505  |
| Z32_mag   | 6.0      | 47.10094   | 95.37684   | 234.132395  | -32.854953 | 7.997970  | 9          | 42.336758  | 8.811306  | 12.439952     | -17.895640 | -37.203135 | 19.863666   | 199.863666  |
| Z33_mag   | 7.0      | 47.10107   | 95.37705   | 250.685156  | -32.176114 | 4.581718  | 8          | 147.172736 | 7.952422  | 6.677876      | -17.462312 | -25.759713 | 7.086542    | 187.086542  |
| Z34_mag   | 8.0      | 47.10111   | 95.37712   | 247.131951  | -35.840117 | 2.844796  | 10         | 289.334789 | 9.963894  | 4.761948      | -19.856873 | -29.843343 | 7.791244    | 187.791244  |
| Z35_mag   | 9.0      | 47.10069   | 95.37747   | 226.181747  | -25.332749 | 6.399180  | 6          | 110.584459 | 5.954786  | 7.702608      | -13.316749 | -38.856026 | 31.001433   | 211.001433  |
| Z36_mag   | 11.0     | 47.10221   | 95.37959   | 247.531592  | -39.317142 | 4.170654  | 8          | 177.361534 | 7.960533  | 6.082124      | -22.208660 | -51.221631 | 5.455763    | 185.455763  |
| Z37_mag   | 12.0     | 47.10221   | 95.37971   | 248.052322  | -42.739898 | 7.478423  | 9          | 48.334733  | 8.834556  | 11.648380     | -24.798438 | -32.562210 | 2.867308    | 182.867308  |
| Z38_mag   | 13.0     | 47.09855   | 95.38445   | 237.351592  | -42.681665 | 8.027422  | 10         | 37.175977  | 9.757908  | 13.284763     | -24.753981 | -39.808772 | 10.899760   | 190.899760  |
| Z39_mag   | 14.0     | 47.09860   | 95.38467   | 230.80551   | -26.400672 | 6.3633220 | 6          | 111.827254 | 5.955288  | 7.659690      | -13.939647 | -36.393048 | 26.087975   | 36.393048   |
| Z40_mag   | 15.0     | 47.09859   | 95.38474   | 241.380972  | -42.753133 | 4.822932  | 9          | 114.937717 | 8.930397  | 7.555335      | -24.808549 | -37.108819 | 7.746124    | 187.746124  |
| Z41_mag   | 10.0     | 47.10109   | 95.37744   | 229.0636998 | -29.074319 | 4.590751  | 8          | 146.532710 | 7.952236  | 6.690955      | -15.536089 | -38.748850 | 206.425574  | 206.425574  |
| Z42_mag   | 16.0     | 47.09577   | 219.192263 | -24.487183  | 11.153830  | 25.622407 | 8          | 25.622407  | 7.728802  | 16.000299     | -12.829071 | -42.668310 | 38.628730   | 218.628730  |
| Z43_mag   | 17.0     | 47.09570   | 95.38638   | 208.946090  | -22.598975 | 10.757156 | 8          | 27.470571  | 7.745182  | 15.454365     | -11.756542 | -47.094786 | 51.278792   | 47.094786   |
| Z44_mag   | 18.0     | 47.09571   | 95.38651   | 160.933464  | -26.16106  | 12.332689 | 5          | 39.445745  | 4.89595   | 12.896888     | 10.052275  | -29.979732 | 297.098874  | 117.098874  |
| Z45_mag   | 19.0     | 47.09562   | 95.38676   | 169.181253  | -22.723096 | 8.151115  | 8          | 47.137245  | 7.851497  | 11.797851     | 11.826377  | -30.288956 | 107.671016  | 287.671016  |
| Z46_mag   | 20.0     | 47.09563   | 95.38692   | 235.938073  | -30.336640 | 6.723891  | 8          | 68.822329  | 7.898289  | 9.763833      | -16.309766 | -34.865831 | 19.680166   | 34.865831   |
| Z47_mag   | 21.0     | 47.09568   | 95.38727   | 236.225390  | -32.077321 | 5.605337  | 8          | 98.607774  | 7.929012  | 8.156981      | -17.399618 | -35.463534 | 18.516120   | 35.463534   |
| Z48_mag   | 22.0     | 47.09574   | 95.38744   | 227.700940  | -32.087392 | 6.771957  | 8          | 67.882078  | 7.898880  | 9.831221      | -17.406005 | -41.018935 | 26.092301   | 41.018935   |
| Z49_mag   | 23.0     | 47.09581   | 95.38747   | 235.973535  | -37.612989 | 9.47951   | 7          | 41.495952  | 6.855420  | 12.573700     | -21.068304 | -38.228444 | 15.487683   | 38.228444   |
| Z50_mag   | 24.0     | 47.09575   | 95.38781   | 175.405740  | 15.829522  | 3.922362  | 8          | 200.402350 | 7.9635070 | 5.721812      | -8.068715  | -34.684493 | 100.922274  | 280.922274  |
| Z51_mag   | 25.0     | 47.09584   | 95.38802   | 229.796663  | -36.494284 | 10.382678 | 5          | 55.264038  | 4.927620  | 10.895915     | -20.299603 | -41.779935 | 21.526652   | 41.779935   |
| Z52_mag   | 26.0     | 47.09583   | 95.38815   | 216.149983  | -45.789543 | 12.698604 | 6          | 28.791577  | 5.826338  | 15.096667     | -27.201966 | -55.462438 | 207.657758  | 207.657758  |
| Z53_mag   | 1.0      | 47.09442   | 95.37205   | 246.701511  | -31.999187 | 3.599051  | 8          | 237.845848 | 7.970569  | 5.252151      | -17.350100 | -28.388510 | 10.165158   | 28.388510   |
| Z54_mag   | 2.0      | 47.09502   | 95.37399   | 243.678159  | -32.414475 | 8.199873  | 8          | 46.589636  | 7.849752  | 11.866984     | -17.613960 | -30.621692 | 12.284724   | 30.621692   |
| Z55_mag   | 3.0      | 47.09525   | 95.37351   | 238.040663  | -33.518307 | 5.611932  | 8          | 98.385329  | 7.928851  | 8.161197      | -18.323455 | -34.914855 | 16.200615   | 34.914855   |
| NaN       | 47.06403 | 181.601802 | 95.42075   | -27.881082  | 5.063905   | 6         | 175.612751 | 5.971528   | 6.112333  | -14.816796    | -57.725144 | 92.519901  | 272.519901  |             |
| NaN       | 47.06227 | 95.42039   | 13.082813  | -31.634060  | 15.516239  | 6         | 27.177964  | 5.816027   | 15.537336 | -17.119456    | -60.043844 | 93.386864  | 273.386864  |             |
| NaN       | 47.06277 | 95.42045   | 119.444412 | -37.602921  | 17.552705  | 6         | 15.519815  | 5.6777831  | 20.560882 | -21.061319    | -35.140582 | 35.140582  | 179.028128  |             |

High-temperature magnetite (tilt-corrected) directions for Teel basalt flows



### Magnetite component VGPs

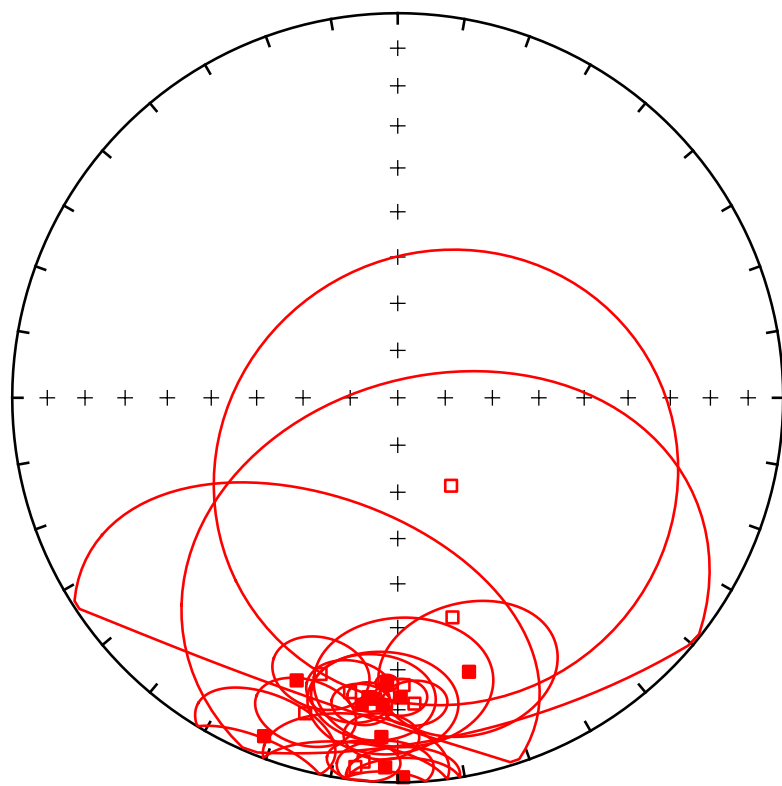


### Hematite directions

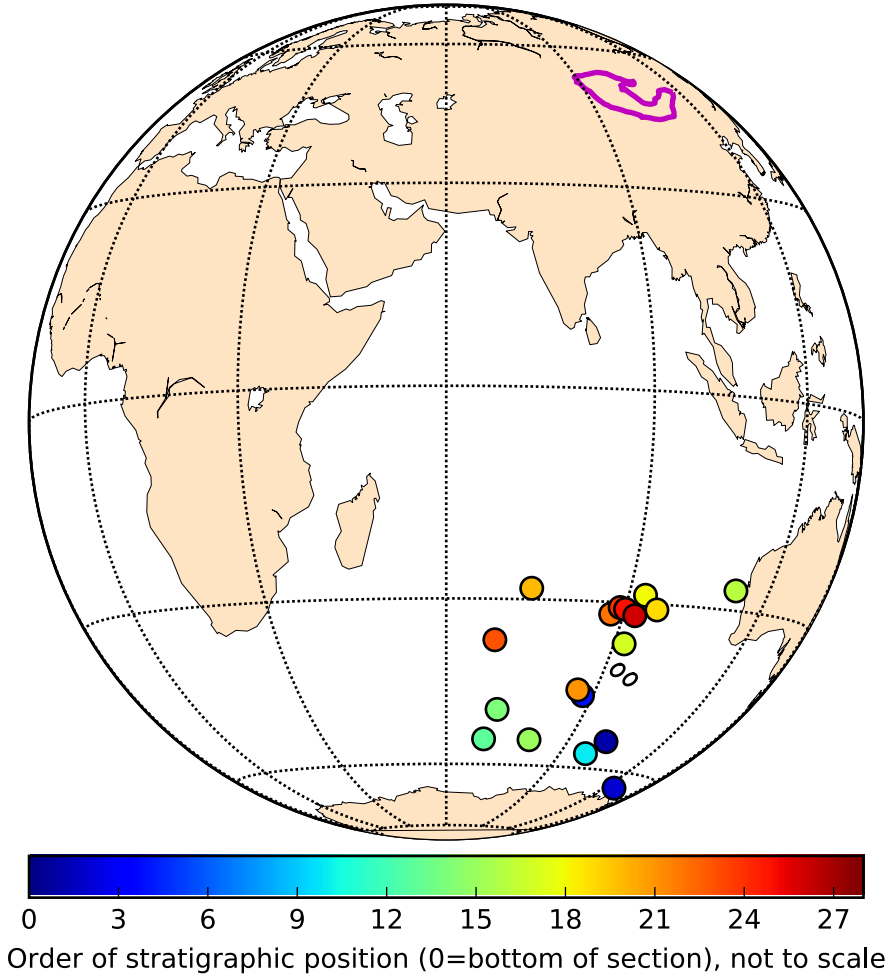
Geographic coordinates - hematite `Out[72]` :

|             | strat_pos | site_lat | site_lon | dec-geo    | inc-geo    | alpha95   | n          | k           | r        | csd        | paleolatitude | vgp_lat    | vgp_lon    | vgp_lat_rev | vgp_lon_rev |
|-------------|-----------|----------|----------|------------|------------|-----------|------------|-------------|----------|------------|---------------|------------|------------|-------------|-------------|
| Z35_hem-geo | 4.0       | 47.10038 | 95.37550 | 185.352162 | -5.560896  | 5.747798  | 6          | 136.842402  | 5.963462 | 6.924281   | -2.787011     | -45.444034 | 87.744611  | 45.444034   | 267.744611  |
| Z30_hem-geo | 9.0       | 47.10069 | 95.37747 | 148.709913 | -68.209834 | 49.957167 | 7          | 2.413452    | 5.13935  | 52.13957   | -69.356099    | -51.356099 | 69.351223  | 208.833918  | 28.833918   |
| Z38_hem-geo | 13.0      | 47.09855 | 95.38445 | 195.565071 | -26.364592 | 8.833229  | 2          | 80.477440   | 1.998752 | 2.861142   | -13.918471    | -13.918471 | 54.362780  | 68.832083   | 248.832083  |
| Z39_hem-geo | 14.0      | 47.09860 | 95.38467 | 196.313095 | -15.623428 | 8.663295  | 5          | 78.962990   | 4.949343 | 9.115347   | -7.959659     | -4.458523  | 70.583219  | 48.458523   | 250.583219  |
| Z40_hem-geo | 15.0      | 47.09859 | 95.38474 | 189.173033 | -23.507115 | 7.794855  | 7          | 60.926778   | 6.901521 | 10.377217  | -12.269627    | -54.326542 | 79.891757  | 54.326542   | 259.891757  |
| Z41_hem-geo | 10.0      | 47.10109 | 95.37744 | 178.834997 | -26.225350 | 16.086290 | 5          | 23.576274   | 4.830338 | 16.681974  | -13.836835    | -5.721476  | 97.439300  | 56.721476   | 277.439300  |
| Z42_hem-geo | 16.0      | 47.09577 | 95.38577 | 165.448451 | -27.278167 | 16.388007 | 6          | 17.664613   | 5.716948 | 19.272274  | -14.457588    | -27.077402 | 111.243174 | 27.077402   | 291.243174  |
| Z43_hem-geo | 17.0      | 47.09571 | 95.38638 | 182.753379 | 12.734651  | 6.220142  | 8          | 80.262873   | 7.912787 | 9.041233   | 6.446942      | -36.401745 | 91.986451  | 36.401745   | 271.986451  |
| Z44_hem-geo | 18.0      | 47.09571 | 95.38651 | 182.138846 | 26.690166  | 2.023836  | 7          | 890.663468  | 6.938263 | 27.14115   | 14.109891     | -28.764330 | 93.029083  | 273.029083  |             |
| Z45_hem-geo | 19.0      | 47.09562 | 95.38676 | 179.431606 | 23.111384  | 4.657126  | 8          | 142.2431974 | 7.950854 | 6.787053   | -30.856760    | 96.034300  | 30.856760  | 276.034300  |             |
| Z46_hem-geo | 20.0      | 47.09563 | 95.38692 | 199.630710 | 23.039855  | 43.076043 | 2          | 35.743651   | 1.972023 | 13.548324  | 73.462329     | -28.348190 | 28.348190  | 253.462329  |             |
| Z47_hem-geo | 21.0      | 47.09568 | 95.38727 | 186.530284 | -3.818259  | 14.407211 | 7          | 18.506577   | 6.675791 | 18.828771  | -1.911251     | 44.460110  | 86.223719  | 44.460110   | 266.223719  |
| Z48_hem-geo | 22.0      | 47.09570 | 95.38744 | 186.680865 | 20.745840  | 5.248580  | 8          | 112.342494  | 7.937691 | 7.642105   | 10.724316     | -31.873027 | 87.651814  | 31.873027   | 267.651814  |
| Z49_hem-geo | 23.0      | 47.09581 | 95.38747 | 195.109581 | 6.066986   | 11.535574 | 6          | 34.086217   | 5.855851 | 13.753288  | -3.042020     | -36.413576 | 68.327763  | 36.413576   | 248.327763  |
| Z50_hem-geo | 24.0      | 47.09575 | 95.38781 | 185.576900 | 22.848691  | 3.695319  | 8          | 225.6633876 | 7.968980 | 5.392051   | 11.897134     | -30.795657 | 89.031882  | 30.795657   | 269.031882  |
| Z51_hem-geo | 25.0      | 47.09584 | 95.38802 | 184.630448 | 22.563173  | 10.926624 | 5          | 49.990867   | 4.919985 | 11.456176  | 11.736415     | -31.022182 | 90.093926  | 31.022182   | 270.093926  |
| Z52_hem-geo | 26.0      | 47.09583 | 95.38815 | 182.777548 | 13.120981  | 21.100104 | 6          | 27.025581   | 5.814990 | 15.581078  | 10.920183     | -31.930956 | 92.174224  | 31.930956   | 272.174224  |
| Z53_hem-geo | 1.0       | 47.09442 | 95.37205 | 176.883446 | 5.750351   | 7         | 11.1157505 | 6.946023    | 7.682731 | -11.116766 | -53.926099    | 100.570110 | 53.926099  | 280.570110  |             |
| Z54_hem-geo | 2.0       | 47.09502 | 95.37299 | 166.032855 | -40.835976 | 52.801938 | 8          | 2.056913    | 4.596843 | 56.477701  | -63.768703    | -23.370939 | 125.457583 | 63.768703   | 305.457583  |
| Z56_hem-geo | NaN       | 47.06403 | 95.42075 | 179.194265 | 1.511589   | 8.593573  | 6          | 61.741195   | 5.919017 | 10.308548  | 0.755926      | -42.174837 | 96.507901  | 42.174837   | 276.507901  |
| Z57_hem-geo | NaN       | 47.06277 | 95.42039 | 181.947932 | 4.332196   | 7.473594  | 4          | 152.109621  | 3.980277 | 6.567600   | 2.169198      | -40.738280 | 92.851012  | 40.738280   | 272.851012  |

Hematite directions from Teel basalt flows in geographic coordinates



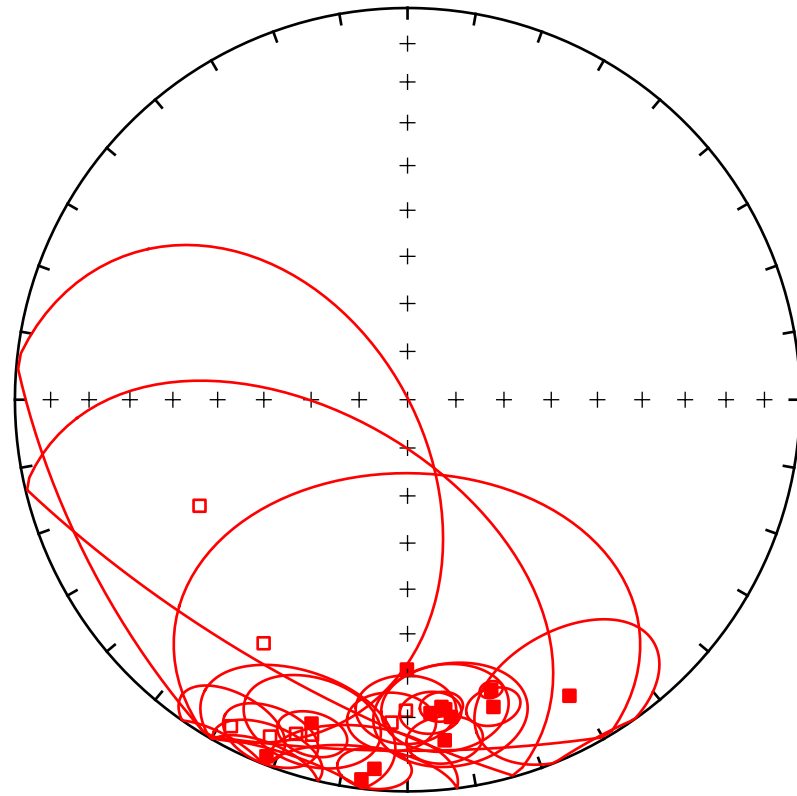
### Hematite (geographic) component VGPs



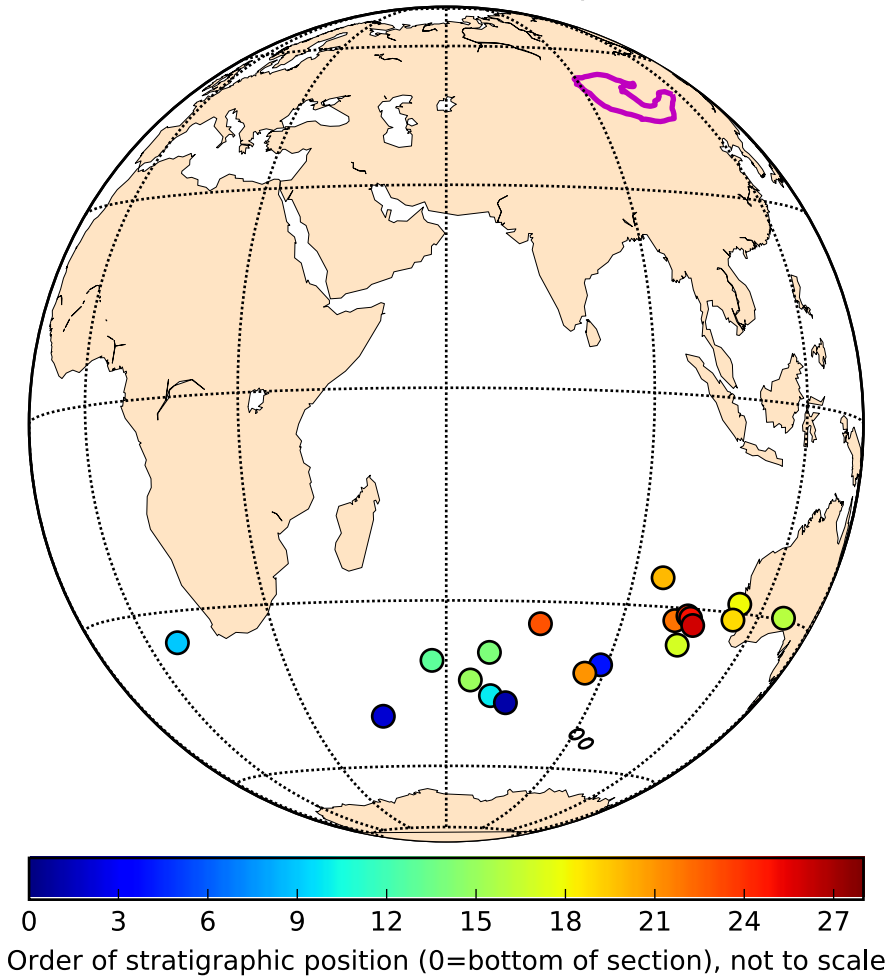
Tilt-corrected coordinates - hematite Out[75]:

|         | strat_pos | site_lat | site_lon   | dec_tc     | inc_tc     | alpha95   | n         | k          | r         | csd        | paleolatitude | vgp_lat      | vgp_lon    | vgp_lat_rev | vgp_lon_rev |
|---------|-----------|----------|------------|------------|------------|-----------|-----------|------------|-----------|------------|---------------|--------------|------------|-------------|-------------|
| Z35_hem | 4.0       | 47.10038 | 95.37550   | 185.114311 | -6.025809  | 5.727598  | 6         | 137.802632 | 5.963716  | 6.900114   | 3.021259      | -39.676603   | 88.733786  | 39.676603   | 268.733786  |
| Z30_hem | 9.0       | 47.10069 | 95.37747   | 242.928054 | -40.237690 | 49.931876 | 7         | 2.414928   | 4.515454  | 52.123423  | -22.933069    | -34.802858   | 188.295178 | 34.802858   | 188.295178  |
| Z38_hem | 13.0      | 47.09855 | 95.38445   | 208.352571 | -5.900502  | 8.908547  | 2         | 788.017587 | 1.399731  | 2.885473   | -2.958094     | -39.503355   | 57.459211  | 39.503355   | 237.459211  |
| Z39_hem | 14.0      | 47.09860 | 95.38467   | 201.539771 | 2.413034   | 8.658960  | 5         | 79.041121  | 4.949333  | 9.110841   | 1.207052      | -38.143076   | 67.563030  | 38.143076   | 247.563030  |
| Z40_hem | 15.0      | 47.09859 | 95.38474   | 202.157748 | -7.928196  | 7.788149  | 7         | 61.030111  | 6.901688  | 10.368429  | -3.983165     | -42.830083   | 64.518459  | 42.830083   | 244.518459  |
| Z41_hem | 10.0      | 47.10109 | 95.37744   | -11.058439 | 16.113432  | 5         | 23.500114 | 4.829788   | 16.708984 | -5.581195  | -45.565273    | 68.698517    | 45.565273  | 248.698517  |             |
| Z42_hem | 16.0      | 47.09577 | 95.38577   | 151.386122 | 14.995751  | 16.374487 | 6         | 17.692229  | 5.717390  | 19.257227  | 7.628503      | -29.676516   | 128.501026 | 29.676516   | 308.501026  |
| Z43_hem | 17.0      | 47.09570 | 95.38638   | 173.787706 | 13.587096  | 6.227989  | 8         | 80.063147  | 7.912569  | 9.052503   | 6.890414      | -35.733259   | 102.991555 | 35.733259   | 282.991555  |
| Z44_hem | 18.0      | 47.09561 | 95.38651   | 103.946455 | 23.981346  | 2.035549  | 7         | 882.184819 | 6.993199  | 12.539568  | -28.658505    | 113.302682   | 28.658505  | 113.302682  | 293.302682  |
| Z45_hem | 19.0      | 47.09562 | 95.38676   | 164.416633 | 19.689336  | 4.663534  | 8         | 141.934618 | 7.950682  | 6.798934   | 10.144077     | -31.097230   | 113.374942 | 31.097230   | 293.374942  |
| Z46_hem | 20.0      | 47.09563 | 95.38692   | 180.134056 | 31.708243  | 43.051197 | 2         | 35.782409  | 1.972053  | 17.166216  | -25.738041    | 95.244729    | 275.244729 | 95.244729   | 275.244729  |
| Z47_hem | 21.0      | 47.09568 | 95.38727   | 186.913270 | 2.679432   | 14.418197 | 7         | 18.470833  | 6.675322  | 18.842390  | 1.340449      | -41.1.8605   | 86.186406  | 41.1.8605   | 266.186406  |
| Z48_hem | 22.0      | 47.09570 | 95.38744   | 175.819816 | 20.880528  | 5.256939  | 8         | 111.988554 | 7.937494  | 7.654172   | 10.798704     | -31.1.985346 | 100.230031 | 31.1.985346 | 280.230031  |
| Z49_hem | 23.0      | 47.09581 | 95.38747   | 196.482372 | 14.863765  | 11.529913 | 6         | 34.719353  | 5.855988  | 7.555953   | -33.419750    | 75.695091    | 33.419750  | 255.695091  | 33.419750   |
| Z50_hem | 24.0      | 47.09581 | 95.38751   | 173.713227 | 22.176830  | 3.699165  | 8         | 225.198841 | 7.969816  | 5.397639   | 11.519700     | -31.1.15698  | 102.38776  | 31.1.15698  | 282.38776   |
| Z51_hem | 25.0      | 47.09584 | 95.38802   | 173.080330 | 21.478208  | 10.923883 | 5         | 50.015473  | 4.920025  | 11.433538  | 11.129977     | -31.446845   | 103.352735 | 31.446845   | 283.352735  |
| Z52_hem | 26.0      | 47.09583 | 95.38815   | 172.236460 | 19.385124  | 13.100041 | 6         | 27.100018  | 5.815560  | 15.557081  | 9.978044      | -32.507612   | 104.465028 | 32.507612   | 284.465028  |
| Z53_hem | 1.0       | 47.09442 | 95.37205   | 195.874742 | -12.092261 | 5.754882  | 7         | 110.984038 | 6.945398  | 7.688733   | -6.114213     | -46.812655   | 71.95627   | 46.812655   | 251.95627   |
| Z54_hem | 2.0       | 47.09502 | 95.37299   | 210.517882 | -28.621488 | 52.793211 | 8         | 2.057276   | 4.397443  | 56.477222  | -15.261779    | -49.341300   | 46.618190  | 49.341300   | 226.618190  |
| NaN     | 47.06403  | 95.42075 | 180.301491 | -21.711722 | 8.592210   | 6         | 61.760484 | 5.919042   | 10.306938 | -11.259937 | -54.195001    | 94.915322    | 54.195001  | 274.915322  |             |
| Z56_hem | NaN       | 47.06277 | 95.42039   | 182.841002 | -18.592084 | 7.462069  | 4         | 152.576865 | 3.980388  | 6.557536   | -9.547317     | -52.406934   | 90.524846  | 52.406934   | 270.524846  |

Hematite (tilt-corrected) directions from Teel basalt flows



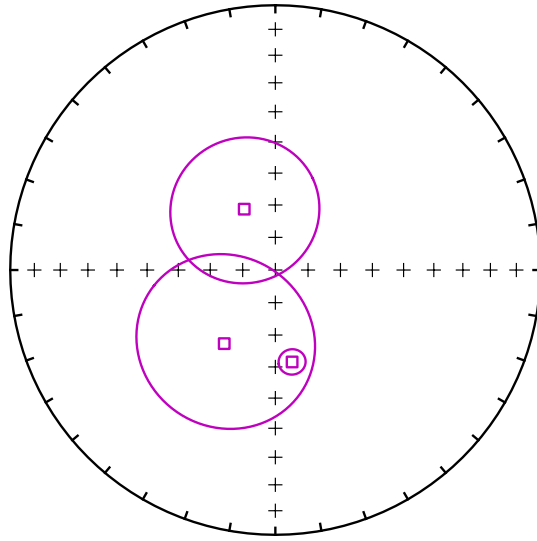
### Hematite (tilt-corrected) component VGPs



Mid-temperature directions [Out\[78\]](#):

|         | strat_pos | site_lat | site_lon | dec_geo    | inc_geo    | alpha95   | n | k          | r        | csd       | paleolatitude | vgp_lat    | vgp_lon    | vgp_lat_rev | vgp_lon_rev |
|---------|-----------|----------|----------|------------|------------|-----------|---|------------|----------|-----------|---------------|------------|------------|-------------|-------------|
| Z42_mid | 16.0      | 47.09577 | 95.38577 | 332.936127 | -68.973663 | 22.704625 | 4 | 17.342624  | 3.827016 | 19.450359 | -52.447527    | -12.194273 | 291.867415 | 12.194273   | 111.867415  |
| Z43_mid | 17.0      | 47.09570 | 95.38638 | 214.749151 | -62.316153 | 27.256978 | 4 | 12.329873  | 3.756688 | 23.067776 | -43.621783    | -65.542782 | 0.679322   | 65.542782   | 180.679322  |
| Z58_mid | NaN       | 47.06277 | 95.42045 | 169.686782 | -61.093602 | 4.004771  | 6 | 280.878503 | 5.982199 | 4.833100  | -42.161138    | -81.183719 | 155.401297 | 81.183719   | 335.401297  |

## Mid-temperature directions from Teel basalt flows in geographic coordinates



Flow Z58 yielded a completely different mid-temperature result compared to all other sites. The magnetite direction is completely different than all other results. The mean direction is very imprecise (SE and moderately-shallow down) but is closest in orientation to the Middle to Late Carboniferous ‘A’ component of Edel et al. (2014).

### 1.5 Paleomagnetic Poles for the Teel Formation

We interpret the primary paleomagnetic direction for the Teel basalts to be held by (titanio)magnetite with a secondary remanence held by hematite holding a distinct direction. However, demagnetization data from some sites within the most oxidized flows show similarities between the remanence directions of magnetite and hematite that correspond to the hematite direction seen in other flows that have a distinct magnetite direction. We suspect that these flows were overprinted in the remagnetization event that led to the hematite overprint. As a result we exclude these flows where magnetite corresponds to the distinct hematite direction from the calculation of the mean magnetite pole.

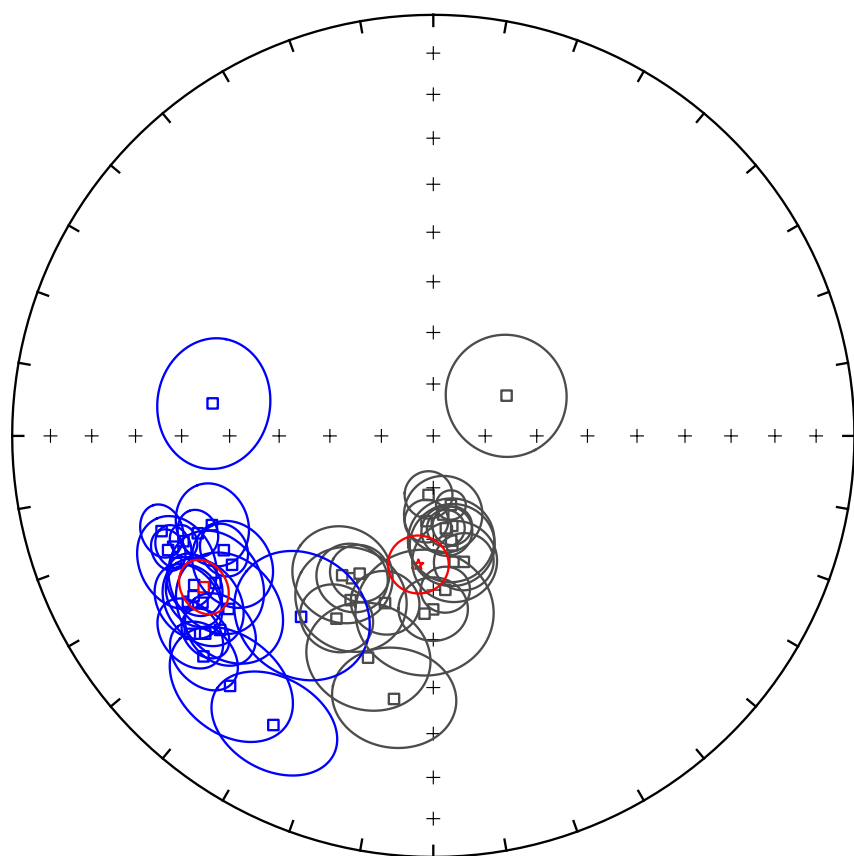
#### Primary magnetite pole - including fold test

```
Out[82]: {'alpha95': 4.9431252055096131,
 'csd': 13.058928417331206,
 'dec': 236.6128693429381,
 'inc': -34.995940978983391,
 'k': 38.472902790170508,
```

```
'n': 23,  
'r': 22.428168960372265}
```

```
Out[83]: {'alpha95': 5.7116821039230583,  
'csd': 15.025346173655382,  
'dec': 186.62753154703333,  
'inc': -64.852074989296611,  
'k': 29.061703291478157,  
'n': 23,  
'r': 22.24299000029874}
```

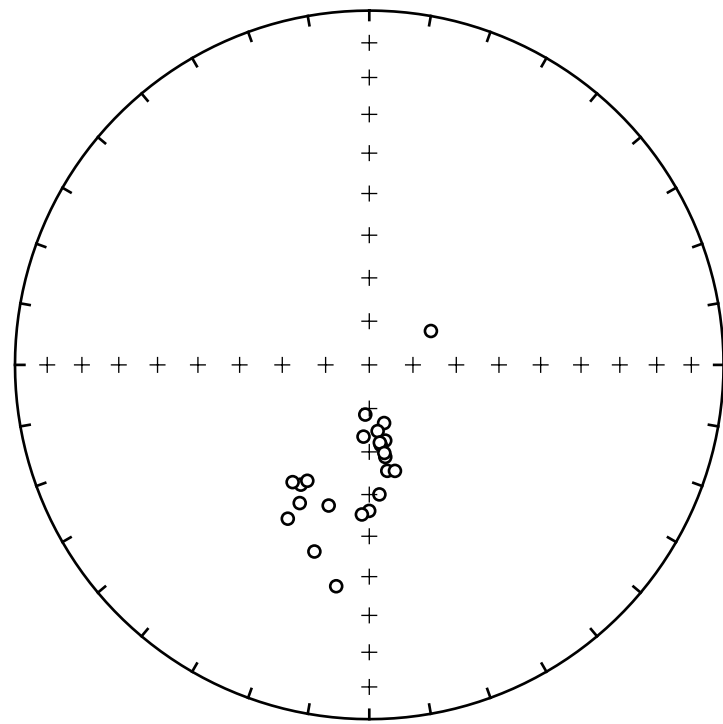
High-temperature magnetite (geographic: gray, tilt-corrected: blue) directions



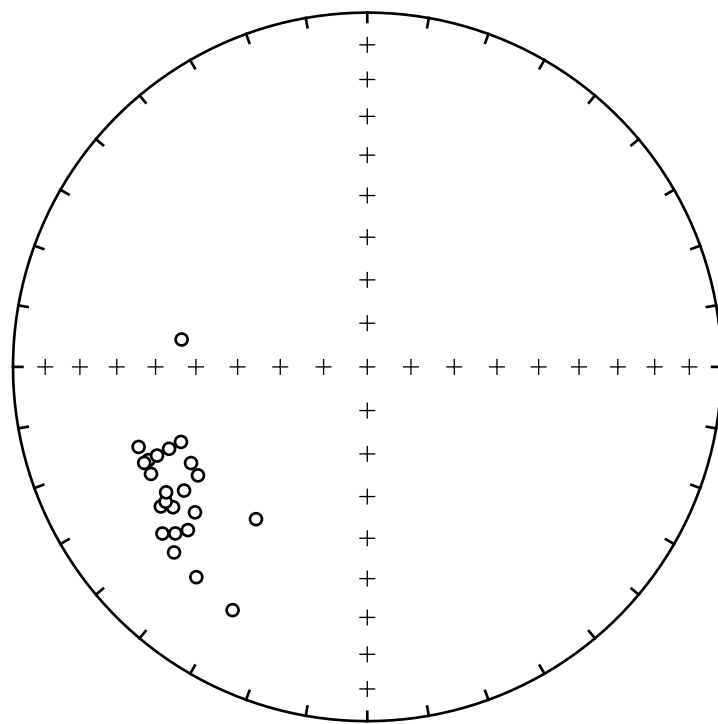
Bootstrap fold test (Tauxe and Watson, 1994)

```
doing 1000 iterations...please be patient...
```

Geographic



Tilt-corrected

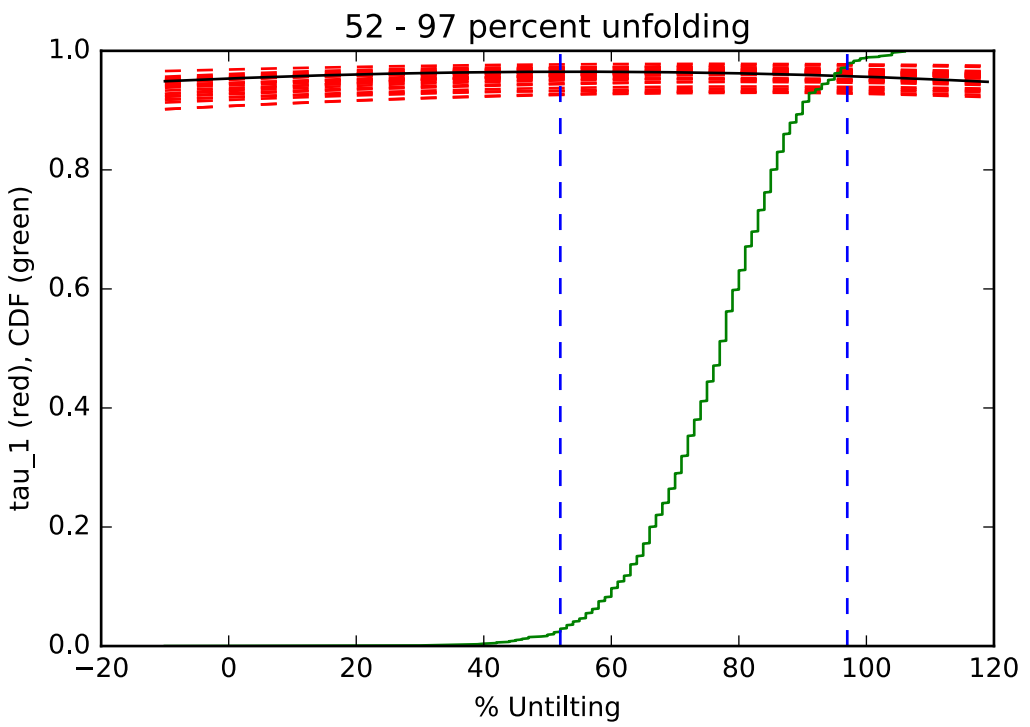


tightest grouping of vectors obtained at (95% confidence bounds):

52 - 97 percent unfolding

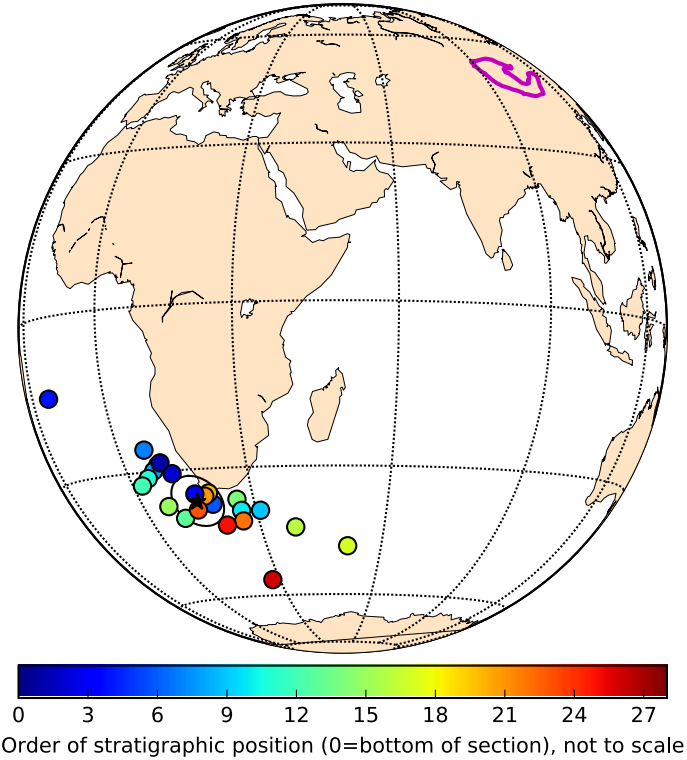
range of all bootstrap samples:

-10 - 106 percent unfolding



Below the tilt-corrected magnetite VGPs are plotted on the globe and shaded according to their relative stratigraphic positions.

Primary magnetite VGPs (excluding those identical to secondary hematite components)

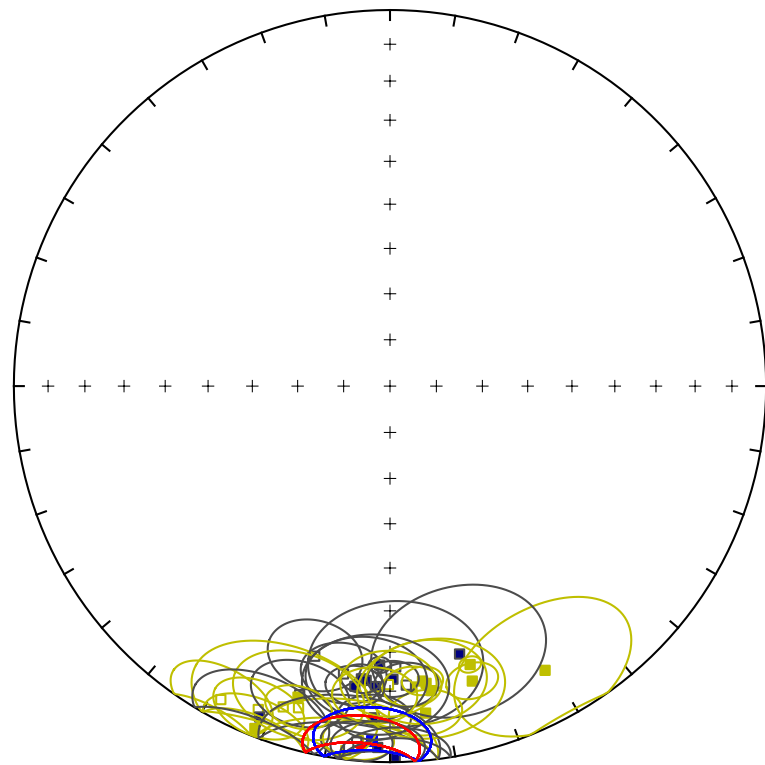


### Secondary hematite pole - including fold test

```
Out[89]: {'alpha95': 9.2608689622177227,
          'csd': 20.97901071644646,
          'dec': 184.58560616364625,
          'inc': 3.8459585385145614,
          'k': 14.907335584818336,
          'n': 18,
          'r': 16.85962183494998}
```

```
Out[90]: {'alpha95': 9.4955663885263011,
          'csd': 21.474669531178204,
          'dec': 182.89089648457883,
          'inc': 6.1094491428847837,
          'k': 14.227122114351561,
          'n': 18,
          'r': 16.805099171613119}
```

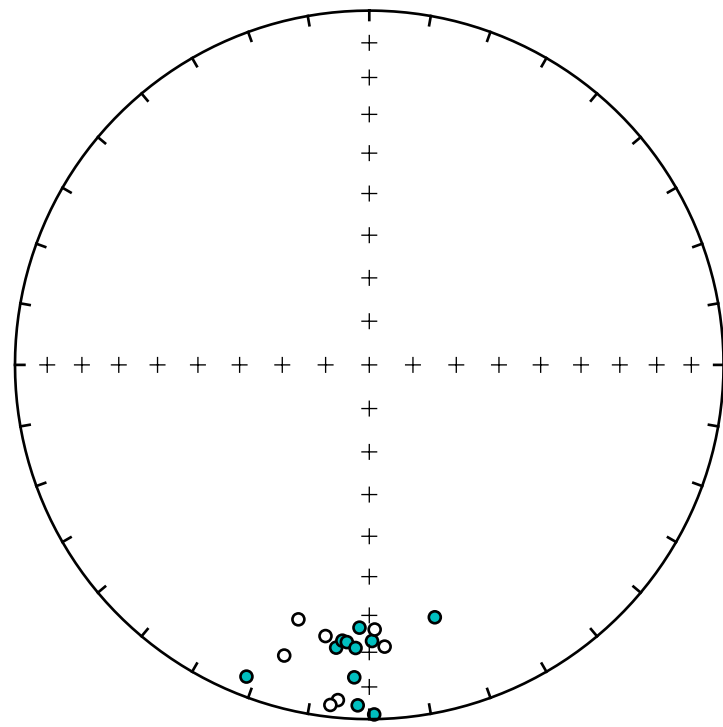
High-temperature hematite (geographic: gray/red, tilt-corrected: yellow/blue) directions



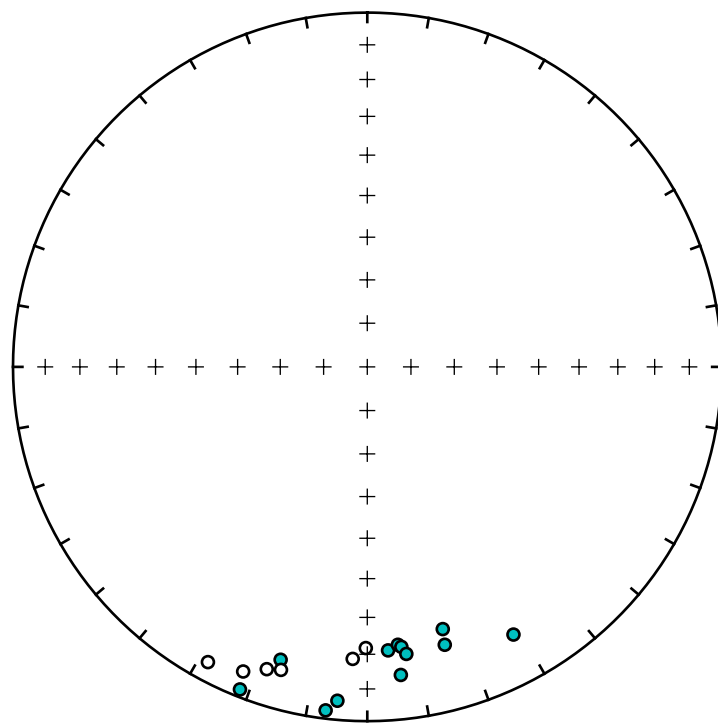
Bootstrap fold test (Tauxe and Watson, 1994)

doing 1000 iterations...please be patient...

Geographic



Tilt-corrected

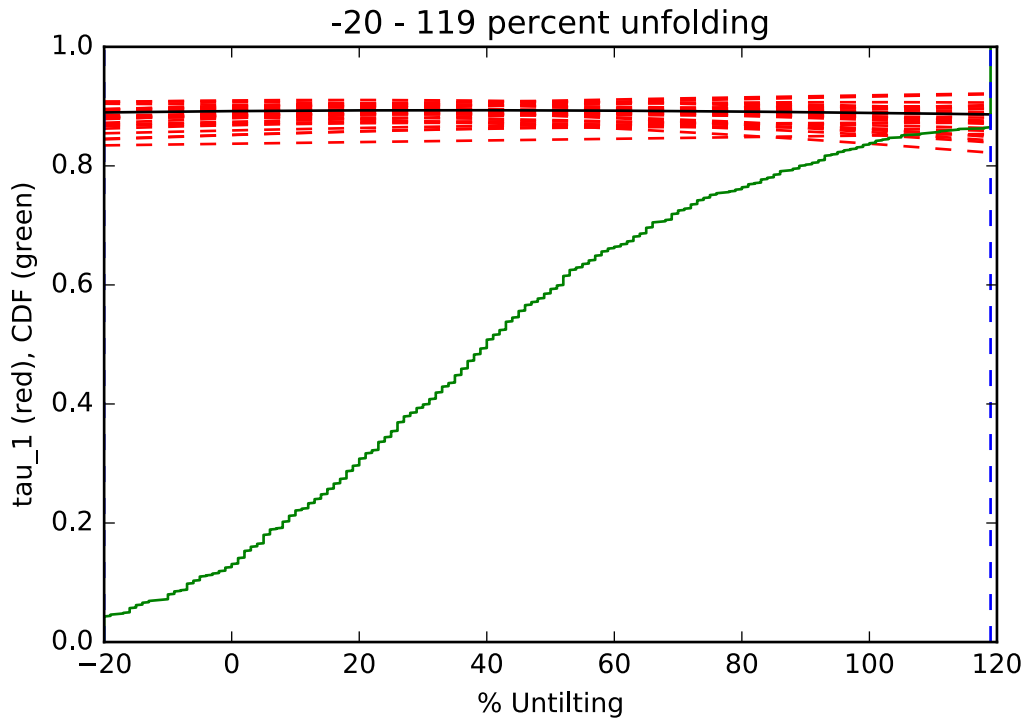


tightest grouping of vectors obtained at (95% confidence bounds):

-20 - 119 percent unfolding

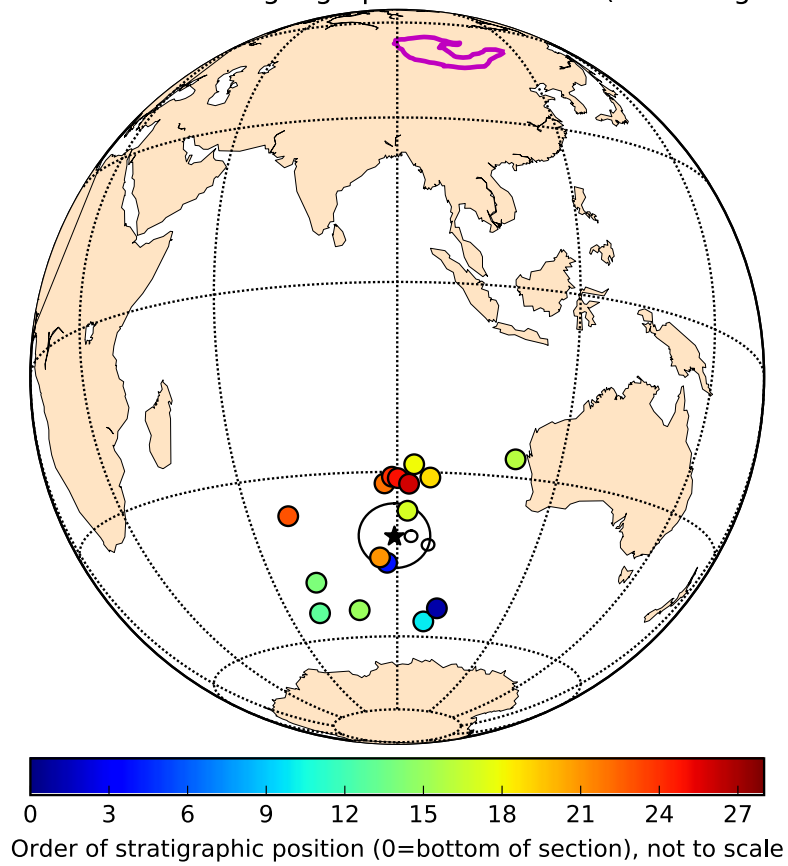
range of all bootstrap samples:

-20 - 119 percent unfolding

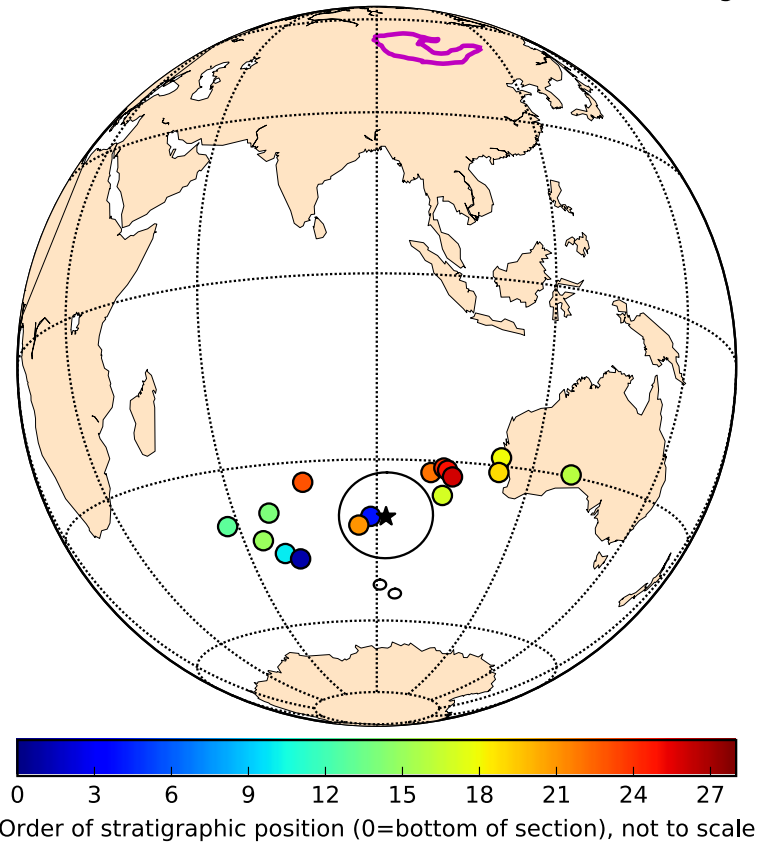


Below the geographic and tilt-corrected hematite VGPs are plotted on the globe and shaded according to their relative stratigraphic positions. Note the similar positions between the two coordinate system means.

Secondary hematite VGPs in geographic coordinates (excluding rhyolite Z30)



Secondary hematite VGPs in tilt-corrected coordinates (excluding rhyolite Z30)



Present local field overprint - negative fold test `Out[95]` :

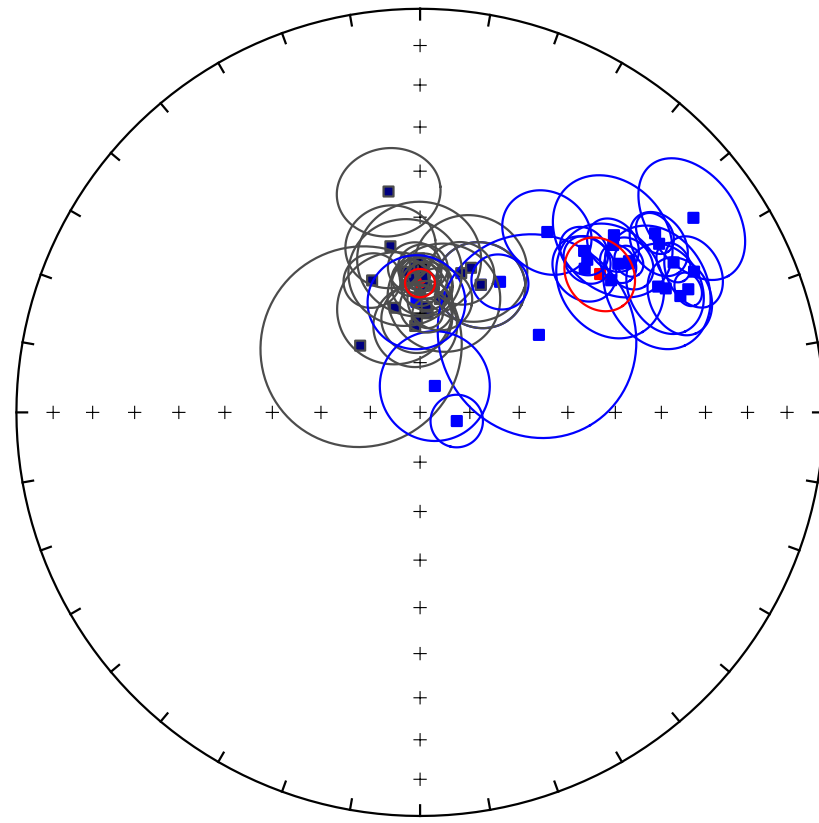
`Out[96]` :

A number of poles are excluded because of inconsistencies between samples within site which resulted in large a95 values for these sites: Z45, Z51, and Z52.

|             | strat_pos | site_lat | site_lon | dec_geo    | inc_geo   | alpha95   | n  | k          | r        | csd       | paleolatitude | vgp_lat   | vgp_lon    | vgp_lat_rev | vgp_lon_rev |
|-------------|-----------|----------|----------|------------|-----------|-----------|----|------------|----------|-----------|---------------|-----------|------------|-------------|-------------|
| Z30_low_geo | 4.0       | 47.10038 | 95.37550 | 346.473053 | 68.261419 | 11.458361 | 7  | 28.705783  | 6.790983 | 15.118208 | 51.429142     | 80.188638 | 36.526238  | -80.188638  | 216.526238  |
| Z31_low_geo | 5.0       | 47.10049 | 95.37604 | 0.054372   | 64.923839 | 3.618073  | 8  | 235.361535 | 7.970259 | 5.279798  | 46.897847     | 89.793993 | 264.986185 | -89.793993  | 84.986185   |
| Z32_low_geo | 6.0       | 47.10094 | 95.37684 | 25.452043  | 61.325382 | 8.812910  | 8  | 40.461392  | 7.826996 | 12.733993 | 42.434489     | 71.428192 | 190.579622 | -71.428192  | 10.579622   |
| Z33_low_geo | 7.0       | 47.10107 | 95.37705 | 0.930272   | 64.380739 | 6.003504  | 8  | 86.089978  | 7.918690 | 8.729889  | 46.196993     | 88.893147 | 239.802233 | -88.893147  | 59.802233   |
| Z34_low_geo | 8.0       | 47.10111 | 95.37712 | 0.648074   | 62.405014 | 3.865736  | 10 | 157.128808 | 9.942722 | 6.461854  | 43.729780     | 86.598151 | 267.460060 | -86.598151  | 87.460060   |

|         | strat_pos | site_lat | site_lon | dec_tc    | inc_tc    | alpha95   | u  | k          | r        | csd       | paleolatitude | vgp_lat   | vgp_lon    | vgp_lat_rev | vgp_lon_rev |
|---------|-----------|----------|----------|-----------|-----------|-----------|----|------------|----------|-----------|---------------|-----------|------------|-------------|-------------|
| Z30_low | 4.0       | 47.10038 | 95.37550 | 62.140855 | 33.713957 | 11.403981 | 7  | 28.680029  | 6.790795 | 15.124935 | 18.450285     | 32.248029 | 192.800152 | -32.248029  | 12.800152   |
| Z31_low | 5.0       | 47.10049 | 95.37604 | 59.403835 | 27.876060 | 3.615270  | 8  | 235.725142 | 7.970304 | 5.275724  | 14.813793     | 31.483537 | 198.002746 | -31.483537  | 18.002746   |
| Z32_low | 6.0       | 47.10094 | 95.37684 | 25.452043 | 61.325382 | 8.812910  | 8  | 40.461392  | 7.826996 | 12.733933 | 42.454489     | 71.428192 | 190.579622 | -71.428192  | 10.579622   |
| Z33_low | 7.0       | 47.10107 | 95.37705 | 54.800714 | 28.344304 | 6.009620  | 8  | 85.916769  | 7.918526 | 8.738684  | 15.094685     | 34.722681 | 201.653195 | -34.722681  | 21.653195   |
| Z34_low | 8.0       | 47.10111 | 95.37712 | 52.688703 | 27.653908 | 3.866823  | 10 | 157.041051 | 9.942690 | 6.463639  | 14.681124     | 35.788473 | 203.849471 | -35.788473  | 23.849471   |

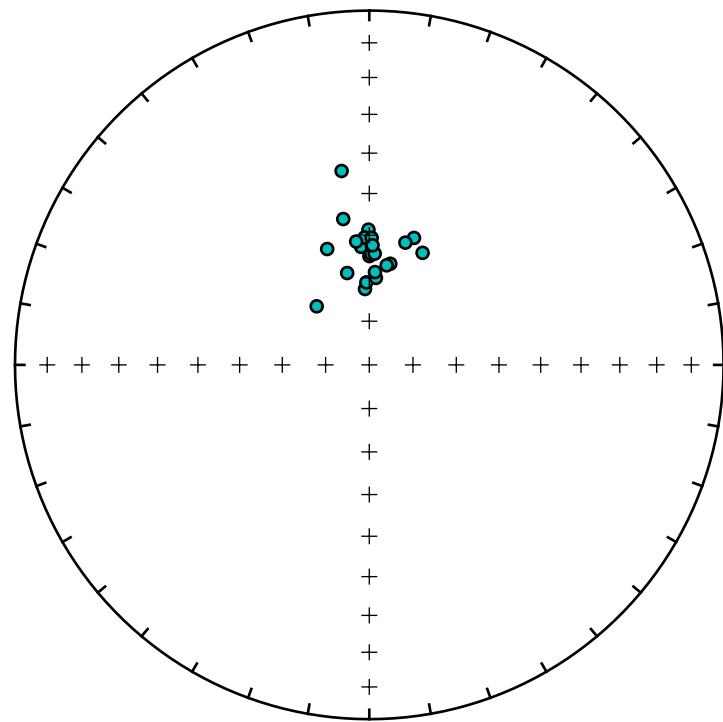
Low-temperature magnetization (geographic: gray, tilt-corrected: blue) directions



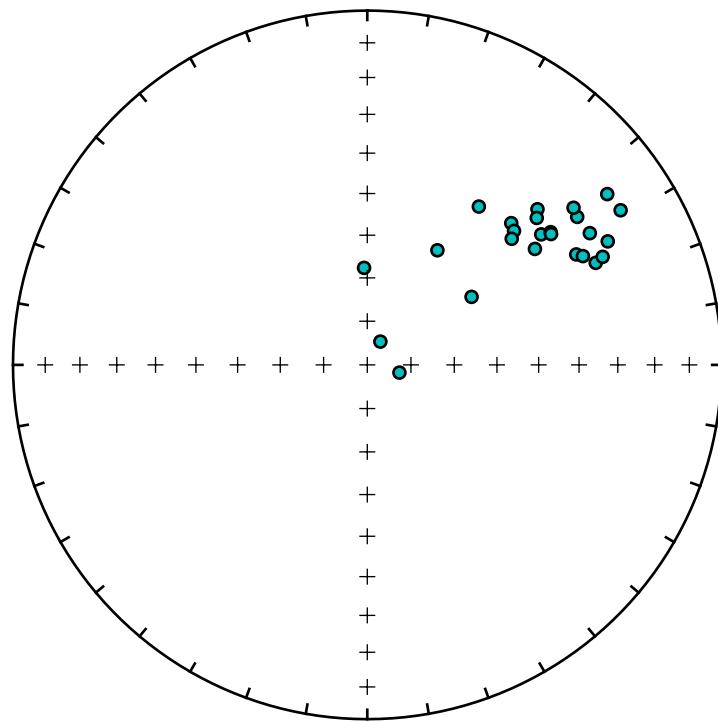
Bootstrap fold test (Tauxe and Watson, 1994)

doing 1000 iterations...please be patient...

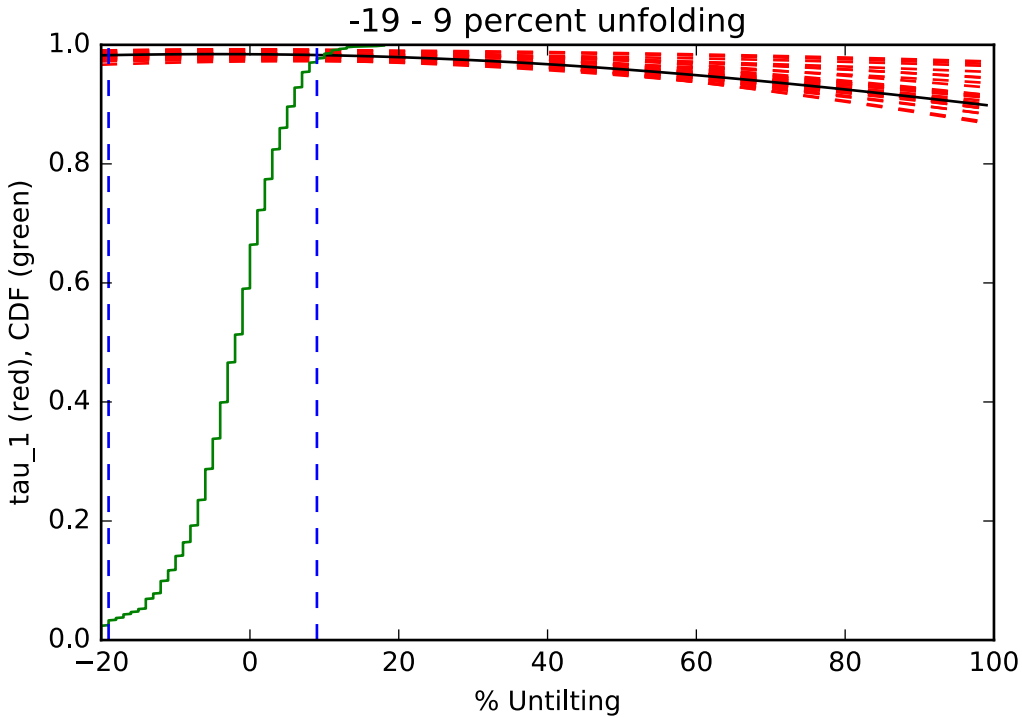
Geographic



Tilt-corrected



tightest grouping of vectors obtained at (95% confidence bounds):  
-19 - 9 percent unfolding  
range of all bootstrap samples:  
-20 - 18 percent unfolding



**Teel poles summary** Out[100]:

|                   | Pole_Lat   | Pole_Long | A_95     | K         | CSD       | N  | r         | Paleolat   |
|-------------------|------------|-----------|----------|-----------|-----------|----|-----------|------------|
| Teel_magnetite_tc | -36.495314 | 16.038788 | 5.236274 | 34.392364 | 13.811918 | 23 | 22.360323 | -19.292649 |
| Teel_hematite_tc  | -39.717588 | 91.918678 | 7.536314 | 22.013320 | 17.264033 | 18 | 17.227740 | 3.063432   |
| Teel_hematite_geo | -40.795648 | 89.426839 | 5.608638 | 38.960325 | 12.976983 | 18 | 17.563659 | 1.925148   |

## 2 Pole compilation for Siberia, North China, and Mongolian terranes

### 2.1 Import existing paleomagnetic data

#### 2.1.1 Siberia

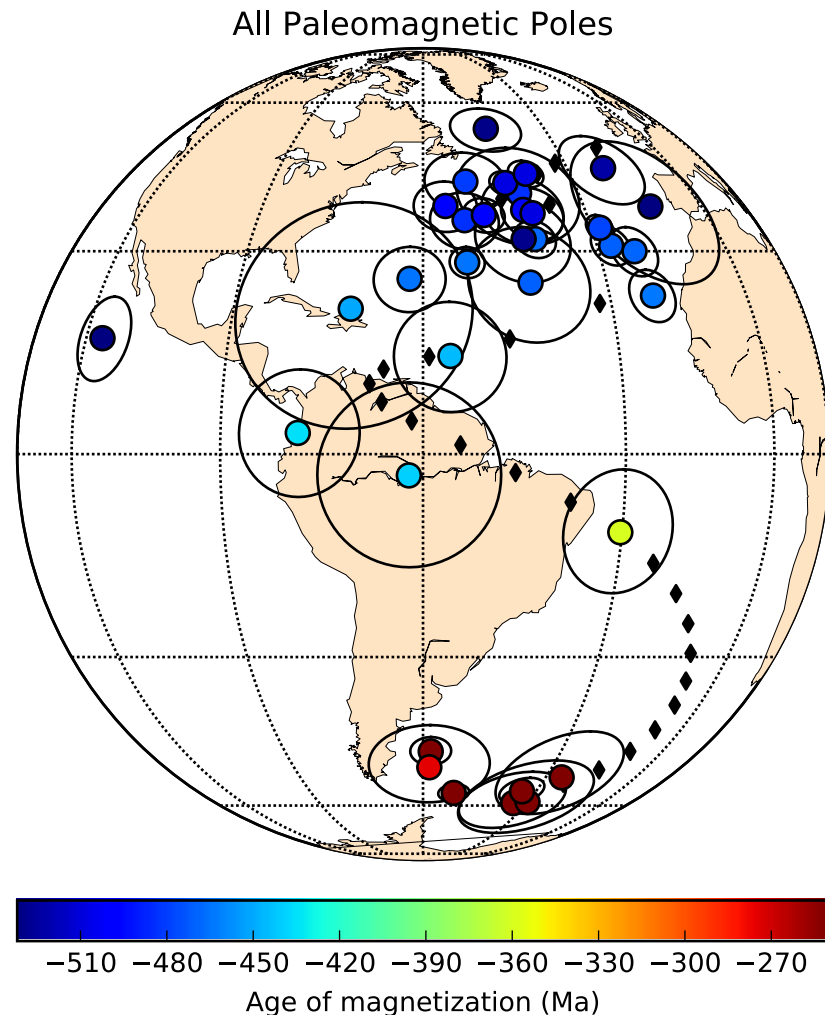
Note that a rotation needs to be applied for relative rotation between Aldan and Anabar blocks before the Devonian Period due to Devonian rifting in the Viljuy Basin near the centre of the craton. Here are two rotations used in the literature: Euler Pole (Lat, Long, rotation)

- (60°N, 120°E, 13°) from Smethurst et al. (1998)
- (60°N, 115°E, 25°) everything pre-Devonian (Evans, 2009)
- (60°N, 120°E, 16°) Cambrian to Early Silurian correction (Cocks and Torsvik, 2007)
- (62°N, 117°E, 20°) pre-Devonian (Pavlov et al. (2008) also used in Powerman et al. (2013))

Most Siberia poles are imported from Cocks and Torsvik (2007) in which the data are rotated from the “southern” Siberia (Aldan) into the northern Siberia (Anabar) reference frame according to Smethurst et al. (1998), which the authors argue brings N and S pre-Devonian poles into the best agreement.

Torsvik et al. (2012) updated their Siberia apparent polar wander path by adding data from Shatsillo et al. (2007) that superceded results from the coeval Lena River sediments (Rodianov et al., 1982; Torsvik et al., 1995). However, there are more results from Siberia that must have been discarded by Cocks and Torsvik (2007) and subsequently by other authors. We discuss these poles later on.

Below we plot the paleomagnetic data compiled by Cocks and Torsvik (2007) for Siberia, shaded according to age.



In the following analyses, we update this pole list to include additional poles from the area in order to construct a paleolatitude plot of Siberia through the Phanerozoic Eon.

We use the Haversine formula to calculate the distance between the VGPs and a reference point on a given plate. This is then used to calculate the paleolatite of the reference point.

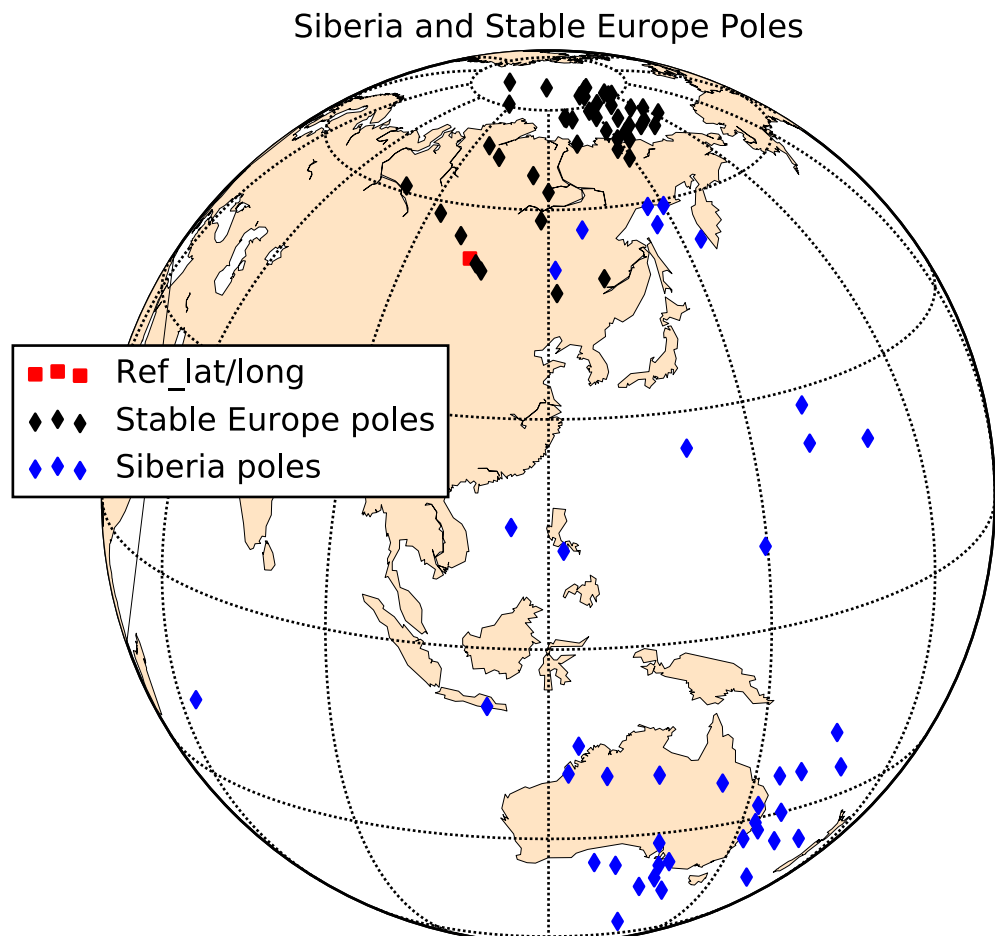
We first load poles for stable Europe from 250 Ma to the present day from Torsvik et al. (2012).

**Out [105] :**

|   | high_age | low_age | median_age | A95  | PLat  | PLon  | Paleolat | PLat_N | PLon_N |
|---|----------|---------|------------|------|-------|-------|----------|--------|--------|
| 0 | 1.0      | 0.0     | 0.5        | 3.6  | -80.6 | 267.5 | 60.638   | 80.6   | 87.5   |
| 1 | 1.0      | 0.0     | 0.5        | 4.4  | -86.4 | 296.1 | 55.206   | 86.4   | 116.1  |
| 2 | 10.0     | 6.0     | 8.0        | 12.9 | -84.3 | 357.7 | 52.907   | 84.3   | 177.7  |
| 3 | 11.0     | 8.0     | 9.5        | 1.8  | -78.9 | 328.3 | 58.733   | 78.9   | 148.3  |
| 4 | 11.0     | 9.0     | 10.0       | 3.5  | -77.4 | 314.2 | 61.900   | 77.4   | 134.2  |

Poles from Siberia are then loaded (545 to 250 Ma). Most of the poles were taken from Cocks and Torsvik (2007) and Torsvik et al. (2012), but we also added additional data gathered from the Global Paleomagnetic Database.

**Out [106] :**



| plate_ID | high_age | low_age | median_age | A95   | PLat  | PLon  | Reference  | Paleolat | PLat_N | PLon_N |
|----------|----------|---------|------------|-------|-------|-------|--|----------|--------|--------|
| 0        | 401      | 245     | 243        | 244.0 | 10.0  | -59.0 | GPDB2832, Gurevitch et al. (1995) from Cocks a...  | 63.178   | 59.0   | 150.0  |
| 1        | 401      | 258     | 238        | 248.0 | 7.8   | -59.3 | Walderhaug et al. (2005) from Cocks and Torsvik... | 65.344   | 59.3   | 145.8  |
| 2        | 401      | 253     | 248        | 251.0 | 3.3   | -56.2 | Gurevitch et al. (2004) from Cocks and Torsvik...  | 65.004   | 56.2   | 146.0  |
| 3        | 401      | 253     | 248        | 251.0 | 9.7   | -52.8 | GPDB3486, Kravchinsky et al. (2002) from Cocks...  | 59.477   | 52.8   | 154.4  |
| 4        | 401      | 253     | 248        | 251.0 | 2.2   | -56.6 | Pavlov and Gallet (1996) from Cocks and Torsvik... | 74.988   | 56.6   | 127.9  |
| 5        | 401      | 285     | 265        | 275.0 | 8.6   | -50.5 | Pisarevsky et al. (2006) from Cocks and Torsvik... | 78.724   | 50.5   | 121.4  |
| 6        | 401      | 363     | 290        | 326.5 | 1.3   | -21.0 | GPDB1991, Davydov and Kravchinsky (1973)           | 30.794   | 21.0   | 170.0  |
| 7        | 401      | 352     | 332        | 342.0 | 17.0  | -16.0 | GPDB1986, Kamysheva (1971)                         | 53.142   | 16.0   | 115.0  |
| 8        | 401      | 348     | 340        | 344.0 | 5.8   | -25.2 | GPDB3041, Zhitkov et al. (1994)                    | 51.715   | 25.2   | 140.0  |
| 9        | 401      | 377     | 350        | 360.0 | 8.9   | -11.1 | GPDB3486, Kravchinsky et al. (2002) from Cocks...  | 34.892   | 11.1   | 149.7  |
| 10       | 401      | 377     | 350        | 363.5 | 10.1  | -27.8 | GPDB3486, Kravchinsky et al. (2002)                | 42.021   | 27.8   | 159.9  |
| 11       | 401      | 377     | 350        | 363.5 | 11.9  | -22.8 | GPDB3486, Kravchinsky et al. (2002)                | 38.641   | 22.8   | 159.4  |
| 12       | 401      | 391     | 363        | 377.0 | -13.0 | 302.0 | GPDB1997, Kamysheva (1975)                         | 48.523   | 13.0   | 122.0  |
| 13       | 410      | 430     | 397        | 413.5 | 3.2   | 8.2   | Powerman et al. (2013)                             | 29.655   | -8.2   | 112.0  |
| 14       | 401      | 443     | 423        | 433.0 | 4.6   | 19.0  | Shatsillo et al. (2007) from Cocks and Torsvik...  | 16.126   | -19.0  | 128.0  |
| 15       | 410      | 444     | 423        | 433.5 | 4.4   | 18.4  | Powerman et al. (2013)                             | 17.919   | -18.4  | 122.7  |
| 16       | 401      | 454     | 424        | 439.0 | 8.0   | 14.0  | Smethurst et al. (1998) from Cocks and Torsvik...  | 21.927   | -14.0  | 124.0  |
| 17       | 401      | 460     | 440        | 450.0 | 17.3  | 19.4  | Smethurst et al. (1998) from Cocks and Torsvik...  | 13.660   | -19.4  | 135.3  |
| 18       | 401      | 461     | 443        | 452.0 | 5.1   | 27.5  | Powerman et al. (2013)                             | 0.109    | -27.5  | 152.0  |
| 19       | 401      | 464     | 444        | 458   | 46.1  | 2.5   | GPDB3473, Iosifidi et al. (1999) from Cocks an...  | 3.312    | -22.8  | 154.2  |
| 20       | 401      | 464     | 444        | 458   | 46.1  | 0.1   | GPDB3473, Iosifidi et al. (1999) from Cocks an...  | 7.787    | -22.1  | 144.9  |
| 21       | 401      | 473     | 453        | 463.0 | 4.0   | 23.0  | Smethurst et al. (1998) from Cocks and Torsvik...  | 1.413    | -23.0  | 158.0  |
| 22       | 401      | 470     | 464        | 467.0 | 3.2   | 30.9  | GPDB3487, Gallet and Pavlov (1998) from Cocks a... | -3.183   | -30.9  | 152.7  |
| 23       | 401      | 478     | 458        | 468.0 | 3.1   | 24.4  | Smethurst et al. (1998) from Cocks and Torsvik...  | -3.645   | -24.4  | 166.0  |
| 24       | 401      | 479     | 459        | 470.0 | 4.0   | 30.0  | Smethurst et al. (1998) from Cocks and Torsvik...  | -4.193   | -30.0  | 157.0  |
| 25       | 401      | 480     | 460        | 470.0 | 9.0   | 17.9  | Smethurst et al. (1998) from Cocks and Torsvik...  | -3.434   | -17.9  | 162.8  |
| 26       | 401      | 488     | 468        | 478.0 | 2.2   | 33.9  | Smethurst et al. (1998) from Cocks and Torsvik...  | -5.441   | -33.9  | 151.7  |
| 27       | 401      | 495     | 470        | 482.5 | 5.8   | 36.2  | GPDB3474, Sunkrik et al. (1999) from Cocks and ... | -10.298  | -36.2  | 158.8  |
| 28       | 401      | 493     | 473        | 483.0 | 9.0   | 40.0  | Smethurst et al. (1998) from Cocks and Torsvik...  | -6.498   | -40.0  | 138.0  |
| 29       | 401      | 495     | 485        | 490.0 | 4.9   | 35.2  | GPDB3448, Gallet and Pavlov (1998) from Cocks ...  | 0.651    | -35.2  | 127.2  |
| 30       | 401      | 495     | 485        | 490.0 | 2.3   | 41.9  | GPDB3192, Pavlov and Gallet (1998) from Cocks ...  | -7.711   | -41.9  | 135.8  |
| 31       | 401      | 510     | 490        | 500.0 | 6.0   | 37.0  | Smethurst et al. (1998) from Cocks and Torsvik...  | -3.690   | -37.0  | 138.0  |
| 32       | 401      | 505     | 495        | 506.0 | 3.0   | 36.1  | GPDB3192, Pavlov and Gallet (1998) from Cocks ...  | -0.974   | -36.1  | 130.7  |
| 33       | 401      | 518     | 495        | 506.5 | 4.5   | 32.6  | GPDB3472, Rodionov et al. (1998) from Cocks an...  | -5.123   | -32.6  | 153.8  |
| 34       | 401      | 514     | 500        | 507.0 | 2.6   | 43.7  | GPDB3537, Gallet et al. (2003) from Cocks and ...  | -10.622  | -43.7  | 140.5  |
| 35       | 401      | 518     | 505        | 511.5 | 4.6   | 36.4  | GPDB3164, Pisarevsky et al. (1997) from Cocks ...  | -3.591   | -36.4  | 139.6  |
| 36       | 401      | 520     | 510        | 515.0 | 5.1   | 53.3  | GPDB3537, Gallet et al. (2003) from Cocks and ...  | -18.264  | -53.3  | 135.0  |
| 37       | 401      | 535     | 518        | 526.5 | 6.8   | 44.8  | GPDB3164, Pisarevsky et al. (1997) from Cocks ...  | -17.577  | -44.8  | 158.7  |
| 38       | 401      | 538     | 518        | 528.0 | 7.0   | 32.0  | Smethurst et al. (1998) from Cocks and Torsvik...  | 1.285    | -32.0  | 137.0  |
| 39       | 401      | 545     | 525        | 535.0 | 6.2   | 16.6  | GPDB1627, Kirschvink and Rozanova (1984) from C... | 13.732   | -16.6  | 64.5   |
| 40       | 401      | 545     | 535        | 540.0 | 12.8  | 37.6  | GPDB3164, Pisarevsky et al. (1997) from Cocks ...  | -14.154  | -37.6  | 165.0  |

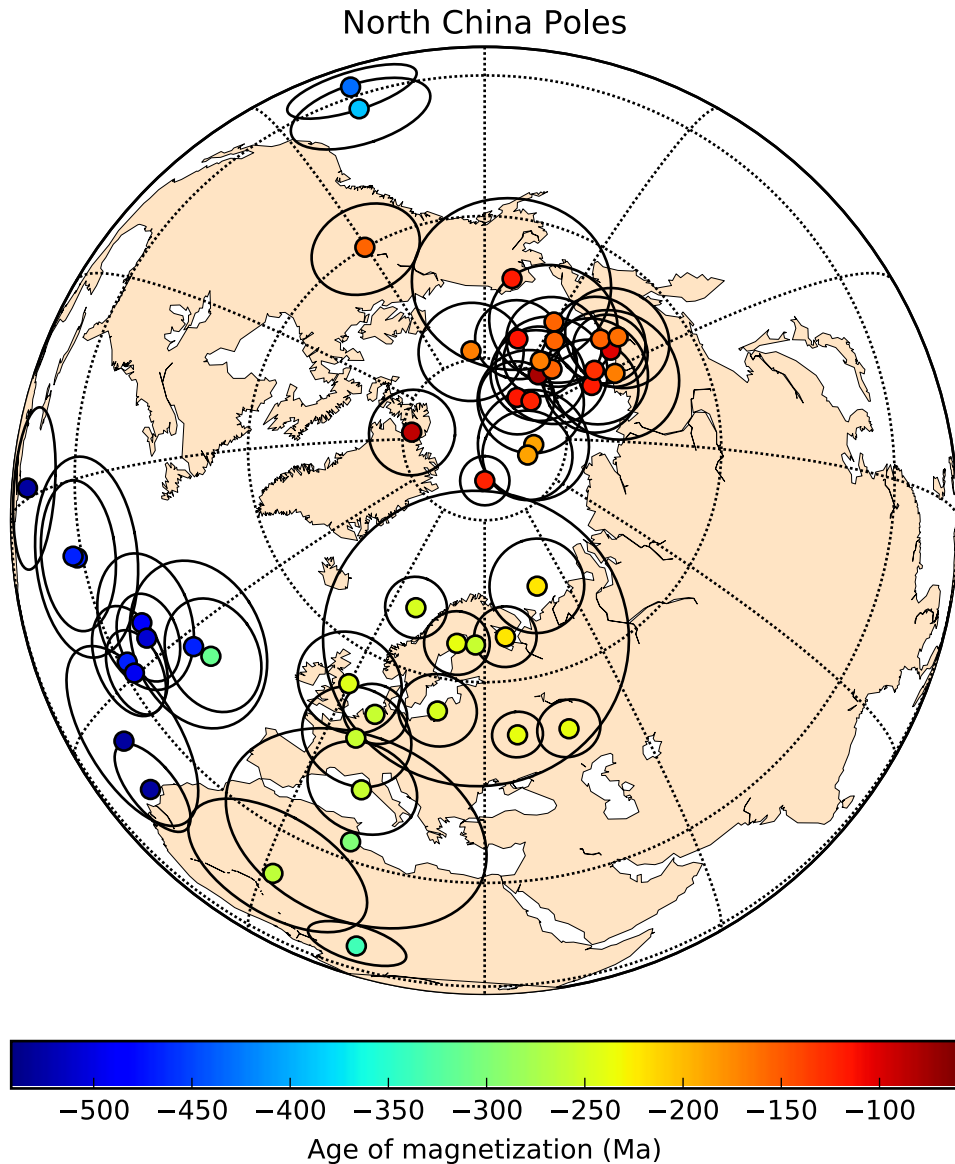
## 2.1.2 North China

We first load the paleomagnetic data for North China compiled in Cocks and Torsvik (2013).

We also add some additional poles from North China that were not included in Cocks and Torsvik (2013) including a compilation of data from Huang et al. (1999) and additional poles from Embleton et al. (1996), Huang et al. (2001), and Doh and Piper (1994).

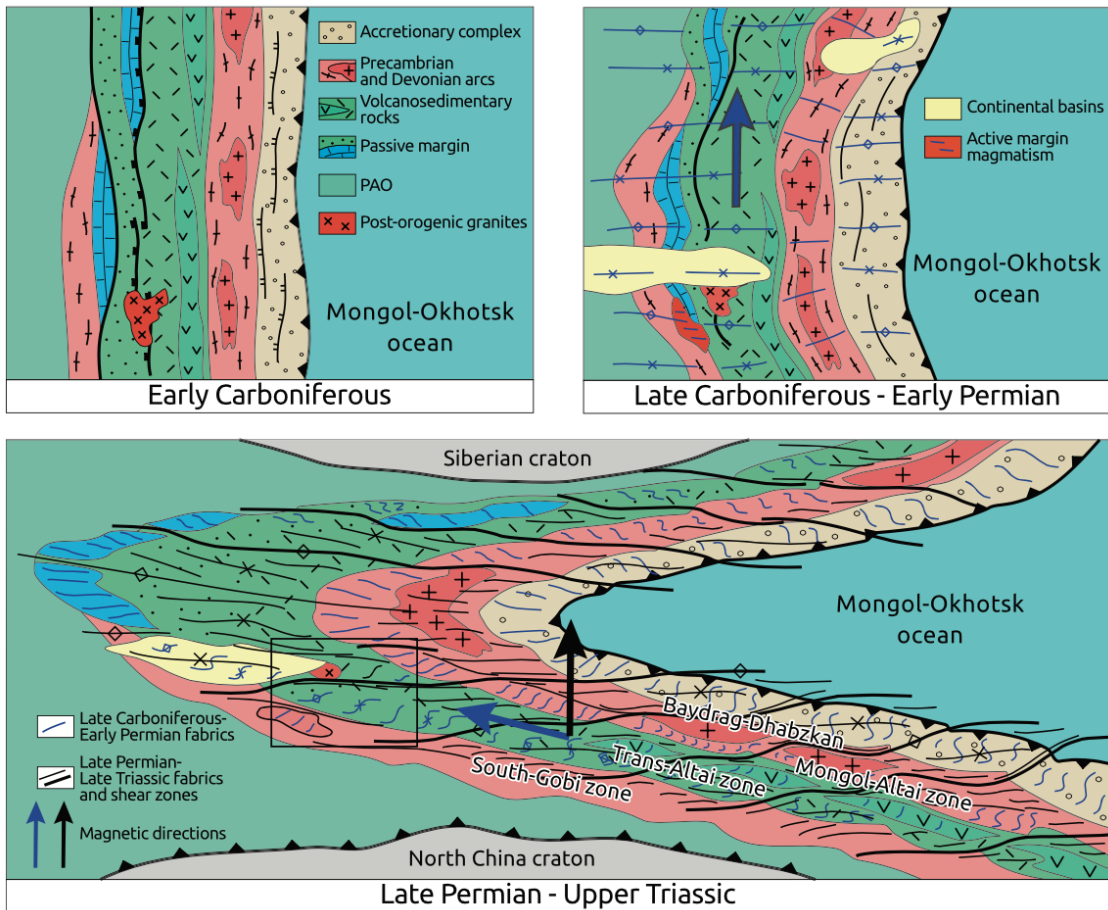
**Out [109]:**

|    | high_age | low_age | median_age | A95  | PLat | PLon  | References                       | Paleolat |
|----|----------|---------|------------|------|------|-------|----------------------------------|----------|
| 0  | 88       | 68      | 78.0       | 5.8  | 79.7 | 170.8 | see Van der Voo et al. (2015)    | 46.149   |
| 1  | 98       | 78      | 88.0       | 5.3  | 81.1 | 294.5 | see Van der Voo et al. (2015)    | 33.136   |
| 2  | 110      | 90      | 100.0      | 4.7  | 70.6 | 156.7 | see Van der Voo et al. (2015)    | 52.870   |
| 3  | 123      | 103     | 113.0      | 5.2  | 76.8 | 192.1 | see Van der Voo et al. (2015)    | 42.209   |
| 4  | 126      | 106     | 116.0      | 4.6  | 83.6 | 172.3 | see Van der Voo et al. (2015)    | 44.602   |
| 5  | 128      | 108     | 118.0      | 5.9  | 75.2 | 147.7 | see Van der Voo et al. (2015)    | 52.663   |
| 6  | 128      | 108     | 118.0      | 12.2 | 69.0 | 200.7 | see Van der Voo et al. (2015)    | 38.082   |
| 7  | 131      | 111     | 121.0      | 3.0  | 84.8 | 30.2  | see Van der Voo et al. (2015)    | 42.801   |
| 8  | 131      | 111     | 121.0      | 6.5  | 82.7 | 159.6 | see Van der Voo et al. (2015)    | 46.356   |
| 9  | 138      | 118     | 128.0      | 6.8  | 73.9 | 153.3 | see Van der Voo et al. (2015)    | 52.221   |
| 10 | 165      | 145     | 155.0      | 6.8  | 59.9 | 240.3 | see Van der Voo et al. (2015)    | 19.446   |
| 11 | 165      | 145     | 155.0      | 7.9  | 72.8 | 180.3 | see Van der Voo et al. (2015)    | 45.207   |
| 12 | 165      | 145     | 155.0      | 5.9  | 74.9 | 175.4 | see Van der Voo et al. (2015)    | 46.347   |
| 13 | 165      | 145     | 155.0      | 6.9  | 78.0 | 166.8 | see Van der Voo et al. (2015)    | 47.463   |
| 14 | 165      | 145     | 155.0      | 5.7  | 70.7 | 162.2 | see Van der Voo et al. (2015)    | 51.138   |
| 15 | 170      | 150     | 160.0      | 6.6  | 68.7 | 159.1 | see Van der Voo et al. (2015)    | 52.805   |
| 16 | 179      | 159     | 169.0      | 8.3  | 71.8 | 148.2 | see Van der Voo et al. (2015)    | 54.640   |
| 17 | 179      | 159     | 169.0      | 6.4  | 78.9 | 218.6 | see Van der Voo et al. (2015)    | 37.490   |
| 18 | 179      | 159     | 169.0      | 4.5  | 78.1 | 175.2 | see Van der Voo et al. (2015)    | 45.774   |
| 19 | 198      | 178     | 188.0      | 6.8  | 84.0 | 112.9 | see Van der Voo et al. (2015)    | 47.985   |
| 20 | 198      | 178     | 188.0      | 5.5  | 84.4 | 98.6  | see Van der Voo et al. (2015)    | 47.499   |
| 21 | 235      | 208     | 221.5      | 5.8  | 70.9 | 49.8  | see Van der Voo et al. (2015)    | 49.184   |
| 22 | 235      | 208     | 221.5      | 3.8  | 65.6 | 36.1  | see Van der Voo et al. (2015)    | 44.398   |
| 23 | 241      | 235     | 238.0      | 4.0  | 64.7 | 22.1  | see Van der Voo et al. (2015)    | 38.471   |
| 24 | 241      | 235     | 238.0      | 3.1  | 52.8 | 36.6  | see Van der Voo et al. (2015)    | 41.977   |
| 25 | 241      | 235     | 238.0      | 3.9  | 52.2 | 46.9  | see Van der Voo et al. (2015)    | 47.889   |
| 26 | 245      | 241     | 243.0      | 6.6  | 55.1 | 359.9 | see Van der Voo et al. (2015)    | 24.183   |
| 27 | 251      | 245     | 248.0      | 3.8  | 67.7 | 7.5   | see Van der Voo et al. (2015)    | 34.254   |
| 28 | 251      | 245     | 248.0      | 4.8  | 55.7 | 19.8  | see Van der Voo et al. (2015)    | 33.960   |
| 29 | 261      | 251     | 256.0      | 18.9 | 64.7 | 27.4  | see Van der Voo et al. (2015)    | 40.643   |
| 30 | 261      | 251     | 256.0      | 6.9  | 48.8 | 5.6   | see Van der Voo et al. (2015)    | 22.956   |
| 31 | 261      | 251     | 256.0      | 4.0  | 52.9 | 7.4   | see Van der Voo et al. (2015)    | 26.331   |
| 32 | 261      | 251     | 256.0      | 6.9  | 42.0 | 9.5   | see Van der Voo et al. (2015)    | 20.891   |
| 33 | 270      | 256     | 263.0      | 12.2 | 20.9 | 1.4   | GPDB3086, Embleton et al. (1996) | 1.649    |
| 34 | 303      | 295     | 299.0      | 16.7 | 33.3 | 10.2  | GPDB3468, Huang et al. (2001)    | 15.804   |
| 35 | 320      | 307     | 313.5      | 7.2  | 44.6 | 335.7 | GPDB2734, Doh and Piper (1994)   | 6.139    |
| 36 | 350      | 321     | 335.5      | 6.2  | 10.5 | 14.0  | GPDB3468, Huang et al. (2001)    | 3.340    |
| 37 | 416      | 360     | 388.0      | 8.8  | 34.2 | 228.7 | see Huang et al. (1999)          | 4.105    |
| 38 | 444      | 416     | 430.0      | 8.2  | 26.2 | 228.4 | see Huang et al. (1999)          | -1.828   |
| 39 | 488      | 444     | 466.0      | 12.3 | 28.8 | 310.9 | see Huang et al. (1999)          | -16.372  |
| 40 | 472      | 461     | 466.5      | 7.0  | 31.5 | 327.7 | Huang et al. (1999)              | -8.331   |
| 41 | 472      | 461     | 466.5      | 10.6 | 43.2 | 332.5 | see Huang et al. (1999)          | 3.732    |
| 42 | 472      | 461     | 466.5      | 9.2  | 27.9 | 310.4 | see Huang et al. (1999)          | -17.360  |
| 43 | 488      | 472     | 480.0      | 8.5  | 37.4 | 324.3 | Huang et al. (1999)              | -4.325   |
| 44 | 501      | 488     | 494.5      | 5.4  | 31.7 | 329.6 | Huang et al. (1999)              | -7.381   |
| 45 | 513      | 501     | 507.0      | 5.5  | 37.0 | 326.7 | Huang et al. (1999)              | -3.836   |
| 46 | 542      | 513     | 527.5      | 6.5  | 18.5 | 341.9 | Huang et al. (1999)              | -12.286  |
| 47 | 542      | 513     | 527.5      | 12.4 | 21.2 | 335.2 | see Huang et al. (1999)          | -13.744  |
| 48 | 542      | 513     | 527.5      | 9.9  | 15.0 | 298.6 | see Huang et al. (1999)          | -32.316  |
| 49 | 542      | 513     | 527.5      | 8.9  | 26.8 | 334.5 | see Huang et al. (1999)          | -9.395   |



### 2.1.3 Mongolia pole compilation

Edel et al. (2014) published paleomagnetic data from 12 sites in the Trans-Altai and South Gobi zones. This work identified magnetic overprint directions for which a variety of arguments are made as to their temporal relationship. The progression of directions as interpreted by the authors leads to an appreciable change in magnetic declination from overprints interpreted to be Middle–Late Carboniferous in age to magnetizations that are interpreted to be Permian in age. The authors propose that this declination change is the result of vertical axis rotation associated with oroclinal bending of a Mongolian ribbon continent (an illustration of this model shown below from that paper).

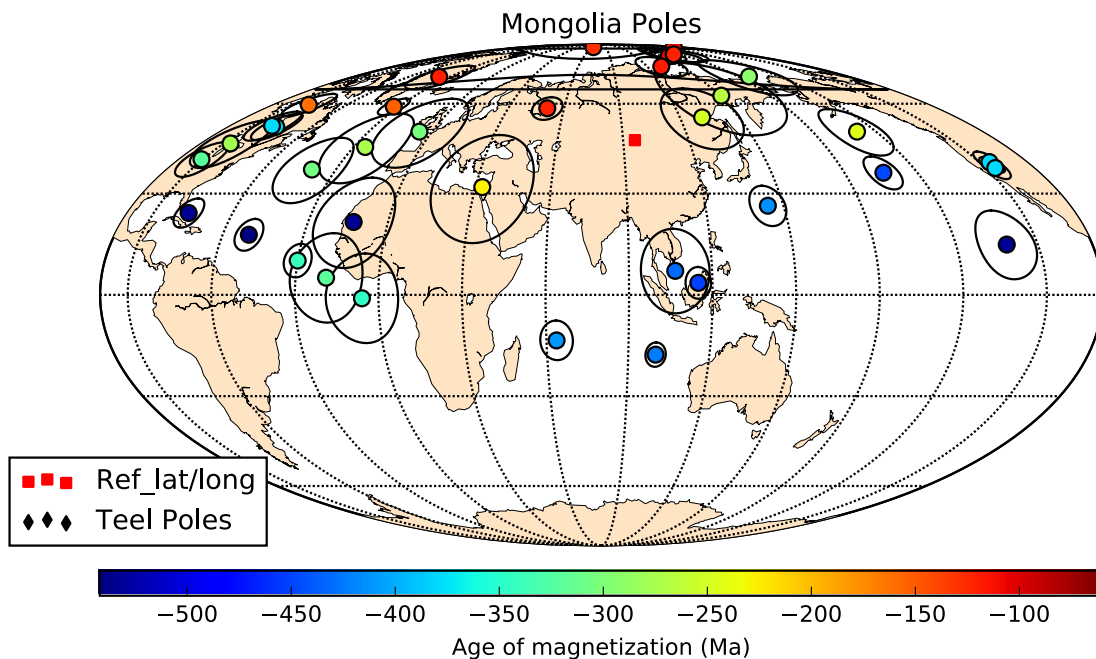


We import paleomagnetic data that have been compiled for Mongolia and some of the surrounding terranes between Siberia and North China and assigned them to established terranes pertinent to this study.

Out [112] :

|    | terrane            | high_age | low_age | median_age | A95  | PLat  | PLon  | Reference                              | Paleolat |
|----|--------------------|----------|---------|------------|------|-------|-------|--|----------|
| 0  | Zavkhan..Baidrag   | 105      | 92      | 98.5       | 3.9  | 81.1  | 165.7 | van Hinsbergen et al. (2008)           | 49.393   |
| 1  | Zavkhan..Baidrag   | 146      | 65      | 105.5      | 21.4 | 86.9  | 252.8 | GPDB2443, Pruner (1992)                | 44.225   |
| 2  | Zavkhan..Baidrag   | 124      | 92      | 108.0      | 2.5  | 80.8  | 158.4 | van Hinsbergen et al. (2008)           | 50.579   |
| 3  | Zavkhan..Baidrag   | 119      | 115     | 117.0      | 4.9  | 75.6  | 132.3 | van Hinsbergen et al. (2008)           | 57.658   |
| 4  | greater..Amuria    | 130      | 110     | 120.0      | 5.2  | 70.8  | 322.4 | Cogne et al. (2005)                    | 32.628   |
| 5  | greater..Amuria    | 145      | 97      | 121.0      | 4.2  | 58.3  | 51.0  | Halim et al. (1998)                    | 61.511   |
| 6  | Zavkhan..Baidrag   | 125      | 118     | 121.5      | 4.3  | 82.0  | 172.3 | van Hinsbergen et al. (2008)           | 48.319   |
| 7  | greater..Amuria    | 133      | 125     | 129.0      | 7.4  | 86.8  | 61.8  | Cogne et al. (2005)                    | 49.735   |
| 8  | greater..Amuria    | 161      | 145     | 153.0      | 3.1  | 58.9  | 327.3 | Cogne et al. (2005)                    | 24.229   |
| 9  | greater..Amuria    | 176      | 145     | 160.5      | 4.2  | 59.6  | 279.0 | Kravchinsky et al. (2002)              | 16.741   |
| 10 | greater..Amuria    | 245      | 208     | 226.5      | 16.8 | 32.0  | 32.7  | GPDB2443, Pruner (1992)                | 40.779   |
| 11 | southern..terranes | 260      | 228     | 244.0      | 8.0  | 50.0  | 201.0 | Edel et al. (2014)                     | 26.317   |
| 12 | Zavkhan..Baidrag   | 260      | 240     | 250.0      | 11.0 | 55.0  | 131.3 | Kovalenko (2010)                       | 66.385   |
| 13 | greater..Amuria    | 271      | 260     | 265.5      | 14.4 | 63.1  | 151.0 | Kravchinsky et al. (2002)              | 55.811   |
| 14 | greater..Amuria    | 290      | 256     | 273.0      | 11.6 | 44.8  | 335.1 | GPDB2443, Pruner (1992)                | 15.820   |
| 15 | southern..terranes | 310      | 245     | 277.5      | 8.0  | 46.0  | 273.0 | Edel et al. (2014)                     | 3.123    |
| 16 | southern..terranes | 300      | 280     | 290.0      | 7.8  | 71.0  | 188.0 | Kovalenko (2010)                       | 43.039   |
| 17 | Zavkhan..Baidrag   | 323      | 290     | 306.5      | 10.4 | 37.5  | 320.1 | GPDB2443, Pruner (1992)                | 3.567    |
| 18 | southern..terranes | 363      | 323     | 343.0      | 13.0 | -1.0  | 354.1 | GPDB3045, Pechersky and Didenko (1995) | -8.390   |
| 19 | southern..terranes | 391      | 363     | 377.0      | 3.4  | 39.9  | 244.3 | GPDB3045, Pechersky and Didenko (1995) | 1.297    |
| 20 | southern..terranes | 391      | 363     | 377.0      | 4.6  | 51.7  | 282.7 | GPDB3045, Pechersky and Didenko (1995) | 8.999    |
| 21 | southern..terranes | 391      | 363     | 377.0      | 3.5  | 38.0  | 244.0 | GPDB2594, Grishin et al. (1991)        | -0.399   |
| 22 | southern..terranes | 391      | 363     | 377.0      | 5.1  | 52.0  | 280.0 | GPDB2594, Grishin et al. (1991)        | 9.179    |
| 23 | southern..terranes | 363      | 245     | 304.0      | 11.9 | 50.0  | 354.0 | GPDB2594, Grishin et al. (1991)        | 28.348   |
| 24 | southern..terranes | 340      | 299     | 319.5      | 13.0 | 5.0   | 341.0 | Edel et al. (2014)                     | -12.479  |
| 25 | Zavkhan..Baidrag   | 440      | 200     | 320.0      | 5.6  | 40.8  | 269.4 | This study                             | -1.939   |
| 26 | southern..terranes | 360      | 320     | 340.0      | 4.9  | 10.0  | 330.0 | Kovalenko (2010)                       | -15.126  |
| 27 | Lake..Zone         | 423      | 397     | 410.0      | 5.8  | -13.3 | 63.7  | Bachtadse et al. (2000)                | 23.280   |
| 28 | Lake..Zone         | 428      | 397     | 412.5      | 6.1  | 26.3  | 144.0 | Bachtadse et al. (2000)                | 46.717   |
| 29 | Lake..Zone         | 428      | 416     | 422.0      | 3.6  | -17.5 | 100.1 | Bachtadse et al. (2000)                | 25.260   |
| 30 | Zavkhan..Baidrag   | 450      | 410     | 430.0      | 12.3 | 7.0   | 106.7 | Kravchinsky (2010)                     | 48.745   |
| 31 | Zavkhan..Baidrag   | 449      | 443     | 446.0      | 5.2  | 36.5  | 196.0 | This study                             | 19.566   |
| 32 | Zavkhan..Baidrag   | 542      | 360     | 451.0      | 4.6  | 3.5   | 114.9 | Evans et al. (1996)                    | 43.245   |
| 33 | Zavkhan..Baidrag   | 545      | 518     | 531.5      | 13.5 | 21.4  | 347.1 | Kravchinsky (2001)                     | 3.927    |
| 34 | Zavkhan..Baidrag   | 545      | 518     | 531.5      | 10.1 | 14.7  | 228.6 | GPDB3045, Pechersky and Didenko (1995) | -15.368  |
| 35 | Zavkhan..Baidrag   | 545      | 518     | 531.5      | 4.4  | 24.1  | 283.3 | GPDB3045, Pechersky and Didenko (1995) | -18.442  |
| 36 | Zavkhan..Baidrag   | 650      | 518     | 584.0      | 4.7  | 17.6  | 309.7 | GPDB3045, Pechersky and Didenko (1995) | -18.324  |
| 37 | Zavkhan..Baidrag   | 650      | 518     | 584.0      | 5.4  | 22.6  | 285.6 | GPDB3045, Pechersky and Didenko (1995) | -19.692  |

Calculate paleolatitudes for the Mongolia poles, considering that many may have experienced horizontal-axis rotations during the formation of the COAB and possibly earlier.

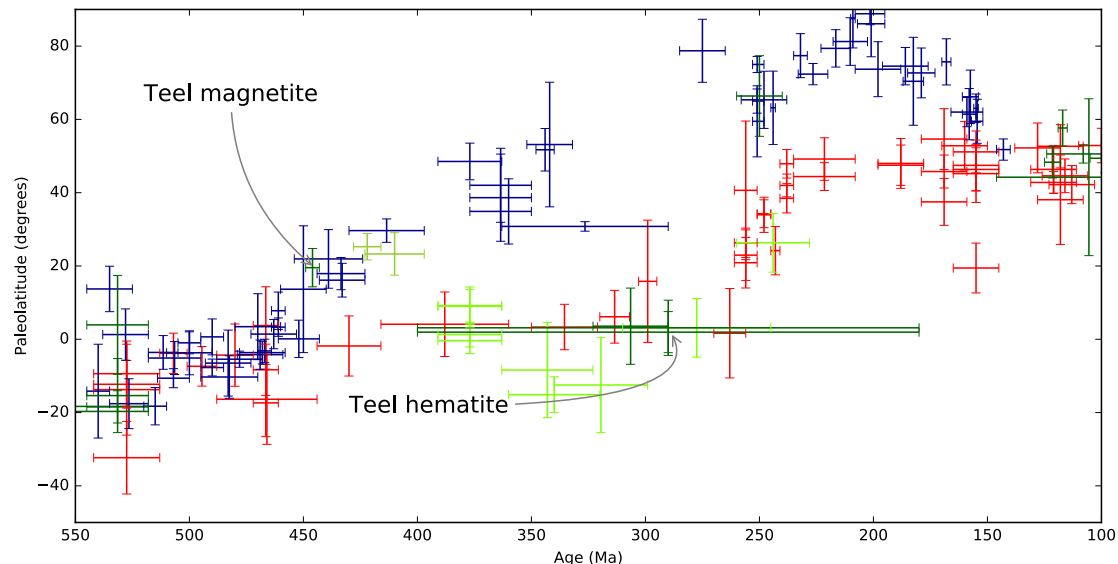


## 2.2 Paleolatitude diagram

We plot the data from Siberia, North China, and Mongolia (from Zavkhan, Baidrag, Lake Zone, and other southern terranes) on a paleolatitude versus time plot. The paleolatitudes given for each block are for specific reference points on each terrane. For Mongolia, the site of the Teel Formation is used ( $95.38^{\circ}\text{N}$ ,  $47.1^{\circ}\text{E}$ ). For Siberia, coordinates at the southern tip of the craton ( $51.7^{\circ}\text{N}$ ,  $103.5^{\circ}\text{E}$ ) are given seeing as this would be the proposed conjugate margin for Mongolia. For North China, a reference point on the northern margin ( $42^{\circ}\text{N}$ ,  $109^{\circ}\text{E}$ ) is given to represent the alternative conjugate margin that would have shared similar paleolatitudes with Mongolia if they were attached.

There are a handful of Mongolian poles that we exclude because of wide age uncertainties or lack of statistical robustness. The Bachtadse et al. (2000) component B pole is excluded because of the small number or samples used to calculate the mean direction (25 samples; unblocking temperatures of  $270\text{--}420^{\circ}\text{C}$ ); it is very similar to two Levashova (2010) directions which may be overprints (see below). The Evans et al. (1996) Bayan-Gol pole was superseded by results from Kravchinsky (2001) and may be a pre-folding overprint, given the increase in precision after tilt correction. The Kravchinsky et al. (2010) pole, that they call a remagnetization, has a very uncertain age and is not tilt-corrected, therefore we see it as unreliable for a paleolatitude estimate. The Kovalenko (2010) pole from the granite at Hanbogd is excluded because it is only from one site and is in the Trans-Altai zone, which is severely affected by early Triassic deformation along the Gobi-Tienshan fault (Lehmann et al., 2010). The “Mongolian sediments and volcanics, Gurvan-Sayhan Range, post-folding” pole from Grishin et al. (1991) (also discussed in Pechersky and Didenko (1995)) is not included because it is likely underaveraged (only from one site) and because of its large age uncertainty; it is also a post-folding remanence.

<matplotlib.figure.Figure at 0x11bb2bcd0>



### 3 Regional overprints in Precambrian rocks

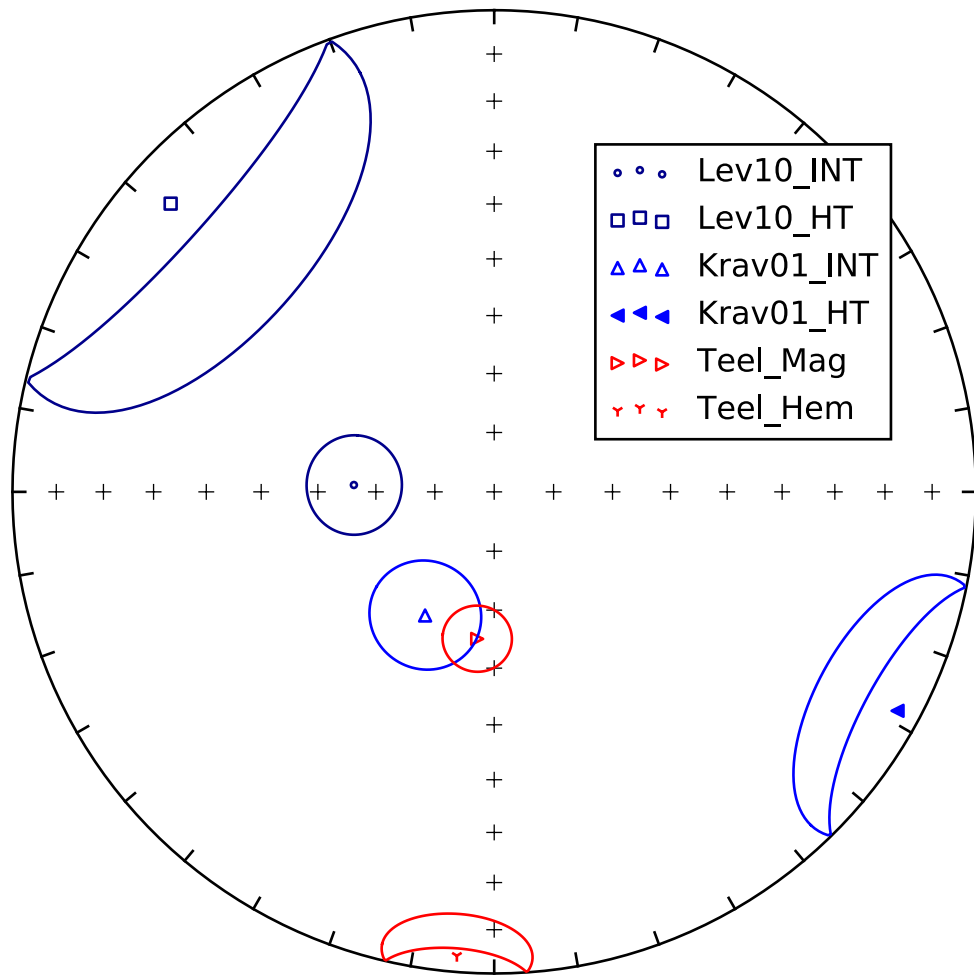
In order to understand the regional paleomagnetic directions, specifically possible overprints, we compare results from the Zavkhan block to see if there are dominant overprints that affected all rocks. These results are from Levashova et al. (2010), Kravchinsky et al. (2001), Evans et al. (1996), this study, and preliminary data from the Zavkhan volcanics.

**Out[117]:**

| ID |              | N   | k_geo | Dec_geo | Inc_geo | a95_geo | k_tc  | Dec_tc | Inc_tc | a95_tc | comments                   |  |
|----|--------------|-----|-------|---------|---------|---------|-------|--------|--------|--------|----------------------------|--|
| 0  | Lev10-INT    | 18  | 19.0  | 272.8   | -66.2   | 8.2     | 3.0   | 158.7  | -42.8  | 24.7   | NaN                        |  |
| 1  | Lev10-HT     | 11  | 3.0   | 311.7   | -11.0   | 30.1    | 19.0  | 321.9  | -65.0  | 10.7   | NaN                        |  |
| 2  | Lev11-INT    | 27  | 14.0  | 207.9   | -30.6   | 7.8     | 6.0   | 210.4  | -4.0   | 12.4   | NaN                        |  |
| 3  | Lev11-HT     | 18  | 10.0  | 194.2   | 29.2    | 11.5    | 41.0  | 179.6  | 53.7   | 5.4    | NaN                        |  |
| 4  | Krav01-LOW   | 10  | 59.7  | 4.1     | 70.9    | 6.3     | 96.8  | 181.2  | 85.6   | 4.9    | data from both B-G and T-O |  |
| 5  | Krav01-INT   | 9   | 31.3  | 209.2   | -66.0   | 9.3     | 117.6 | 284.3  | -79.7  | 4.8    | data from both B-G and T-O |  |
| 6  | Krav01-HT    | 6   | 14.9  | 118.5   | 5.3     | 17.9    | 13.3  | 118.3  | -6.3   | 19.0   | data from B-G              |  |
| 7  | Teel_mag     | 23  | 29.1  | 186.6   | -64.9   | 5.7     | 38.5  | 236.6  | -35.0  | 4.9    | NaN                        |  |
| 8  | Teel_hem     | 18  | 14.9  | 184.6   | 3.8     | 9.3     | 14.2  | 182.9  | 6.1    | 9.5    | NaN                        |  |
| 9  | Evans_HT     | 193 | NaN   | NaN     | NaN     | NaN     | 5.8   | 331.9  | -62.6  | 4.6    | NaN                        |  |
| 10 | Z09_cgl.INT  | 20  | 32.3  | 200.7   | -62.2   | 5.8     | 32.3  | 212.3  | -5.8   | 5.8    | NaN                        |  |
| 11 | Z104_cgl.INT | 31  | 165.4 | 174.8   | -61.7   | 2.0     | 165.2 | 61.9   | -71.4  | 2.0    | NaN                        |  |

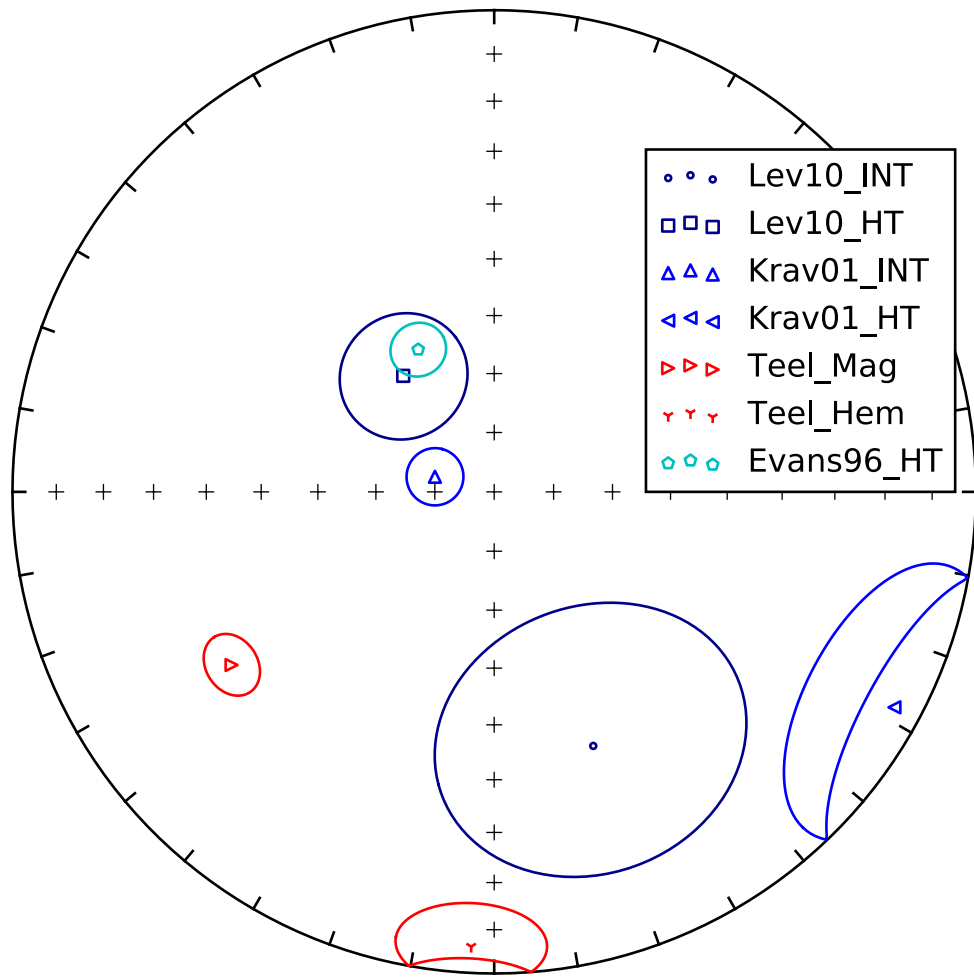
All directions are first plotted in geographic coordinates.

### Overprint Directions - GEOGRAPHIC COORDS.



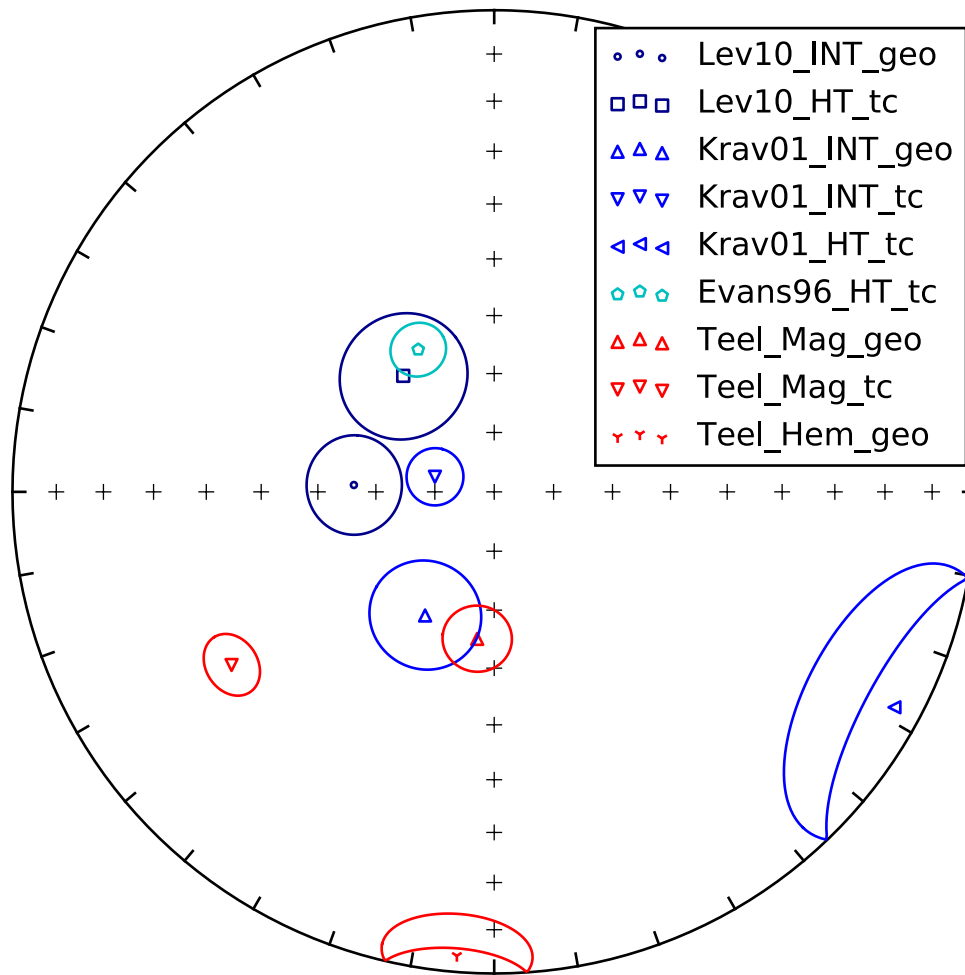
Then the overprint data are plotted in tilt-corrected coordinates.

### Overprint Directions - Tilt-Corrected



Given geological and statistical paleomagnetic context (improvement during tilt correction) we create a plot of what we consider to be the overprint directions if they were acquired either before or after folding.

### Overprint Directions - geographic/tilt-corrected



As stated in the main text, the Kravchinsky et al. (2001) intermediate component from late Neoproterozoic to early Cambrian in geographic coordinates is similar to the Teel magnetite component in geographic coordinates. It is possible that the Ordovician magmatism recorded in the Teel Formation basalts caused this overprint in older lithologies.

## 4 Data Repository References

Bachtadse, V., Pavlov, V. E., Kazansky, A. Y., and Tait, J. A., 2000, Siluro-Devonian paleomagnetic results from the Tuva Terrane (southern Siberia, Russia): implications for the paleogeography of Siberia: Journal of Geophysical Research: Solid Earth, vol. 105, pp. 13,509-13,518,

doi:10.1029/1999JB900429.

Cogne, J.-P., Kravchinsky, V. A., Halim, N., and Hankard, F., 2005, Late Jurassic-Early Cretaceous closure of the Mongol-Okhotsk Ocean demonstrated by new Mesozoic palaeomagnetic results from the Trans-Baikal area (SE Siberia): *Geophysical Journal International*, vol. 163, pp. 813-832, doi:10.1111/j.1365-246X.2005.02782.x.

Edel, J. B., Schulmann, K., Hanzl, P., and Lexa, O., 2014, Palaeomagnetic and structural constraints on 90° anticlockwise rotation in SW Mongolia during the Permo-Triassic: Implications for Altaiid oroclinal bending. Preliminary palaeomagnetic results: *Journal of Asian Earth Sciences*, vol. 94, pp. 157-171, doi:10.1016/j.jseas.2014.07.039.

Evans, D. A., Zhuravlev, A. Y., Budney, C. J., and Kirschvink, J. L., 1996, Palaeomagnetism of the Bayan Gol Formation, western Mongolia: *Geological Magazine*, vol. 133, pp. 487-496.

Grishin, D., Didenko, A., Pechersky, D., and T.L., T., 1991, [Paleomagnetic study and petromagnetic study of structure and evolution of paleoceanic lithosphere (Phanerozoic ophiolites of Asia)] (in Russian), VNIGRI, Leningrad, Russia, pp. 135-149.

Halim, N., Kravchinsky, V., Gilder, S., Cogne, J.-P., Alexyutin, M., Sorokin, A., Courtillot, V., and Chen, Y., 1998, A palaeomagnetic study from the Mongol-Okhotsk region: rotated Early Cretaceous volcanics and remagnetized Mesozoic sediments: *Earth and Planetary Science Letters*, vol. 159, pp. 133-145, doi:10.1016/S0012-821X(98)00072-7.

Kovalenko, D., 2010, Paleomagnetism of Late Paleozoic, Mesozoic, and Cenozoic rocks in Mongolia: *Russian Geology and Geophysics*, vol. 51, pp. 387-403, doi:10.1016/j.rgg.2010.03.006.

Kravchinsky, V., Konstantinov, K., and Conge, J., 2001, Palaeomagnetic study of Vendian and Early Cambrian rocks of South Siberia and Central Mongolia: Was the Siberian platform assembled at this time?: *Precambrian Research*, vol. 110, pp. 61-92.

Kravchinsky, V. A., Cogne, J.-P., Harbert, W. P., and Kuzmin, M. I., 2002, Evolution of the Mongol-Okhotsk Ocean as constrained by new palaeomagnetic data from the Mongol-Okhotsk suture zone, Siberia: *Geophysical Journal International*, vol. 148, pp. 34-57.

Kravchinsky, V. A., Sklyarov, E. V., Gladkochub, D. P., and Harbert, W. P., 2010, Paleomagnetism of the Precambrian Eastern Sayan rocks: Implications for the Ediacaran-Early Cambrian paleogeography of the Tuva-Mongolian composite terrane: *Tectonophysics*, vol. 486, pp. 65-80, doi:10.1016/j.tecto.2010.02.010.

Pechersky, D. and Didenko, A., 1995, Paleo-Asian Ocean (in Russian): United Institute of Earth's Physics Publ., Moscow, 298 pp.

Pruner, P., 1992, Palaeomagnetism and palaeogeography of Mongolia from the Carboniferous to the Cretaceous - final report: *Physics of the Earth and Planetary Interiors*, vol. 70, pp. 169-177, doi:10.1016/0031-9201(92)90179-Y.

Van Hinsbergen, D. J. J., Straathof, G. B., Kuiper, K. F., Cunningham, W. D., and Wijbrans, J., 2008, No vertical axis rotations during Neogene transpressional orogeny in the NE Gobi Altai: coinciding Mongolian and Eurasian early Cretaceous apparent polar wander paths: *Geophysical Journal International*, vol. 173, pp. 105-126, doi:10.1111/j.1365-246X.2007.03712.x.